Hindawi
Structural Control and Health Monitoring
Volume 2023, Article ID 4024741, 22 pages
https://doi.org/10.1155/2023/4024741

Research Article

Stochastic Optimization and Sensitivity Analysis of the Combined Negative Stiffness Damped Outrigger and Conventional Damped Outrigger Systems Subjected to Nonstationary Seismic Excitation

Zhihao Wang,[1] **Yuxiang Zhou**,[1] **Chuangjie Fang**,[2] **and Jingwen Zhang**[1]

[1]*School of Civil Engineering and Communication, North China University of Water Resources and Electric Power, Zhengzhou, China*
[2]*Department of Civil and Environmental Engineering, Shantou University, Shantou 515063, Guangdong, China*

Correspondence should be addressed to Chuangjie Fang; cjfang@outlook.com

Received 26 October 2022; Revised 6 January 2023; Accepted 11 January 2023; Published 8 February 2023

Academic Editor: Chia-Ming Chang

In recent years, various kinds of damped outrigger systems, particularly with the negative stiffness devices, have been shown to effectively suppress excessive vibration induced by earthquake and wind. To gain insight into such systems, this paper proposes a stochastic optimization method to investigate optimal configurations of combined negative stiffness damped outriggers (NSDOs) and conventional damped outriggers (CDOs) subjected to nonstationary stochastic seismic excitation. The simplified analysis model of various combinations of damped outriggers is developed, and the state-space representation of outrigger systems is then formulated. The nonstationary seismic excitation is modeled as a uniformly modulated stationary Gaussian process with a time-modulating function following Clough–Penzien spectrum, and combining equations of motions of outrigger systems and seismic excitation gives rise to the augmented state-space representation of structure-damper-excitation and subsequently the differential Lyapunov equation. The optimal designs of damped outriggers are defined via the solution of the differential Lyapunov equation. The multiobjective optimization with Pareto optimal fronts is adopted to deal with conflicting objectives between harmful interstory drift and floor absolute acceleration. The sensitivity of negative stiffness devices on optimal objectives is also investigated. The optimal designs are further examined under real typical and near-fault earthquake records. The results demonstrate the efficacy of the proposed method and provide insight into the systems subjected to nonstationary seismic excitation. While the purely NSDO systems could have better performance with adequate negative stiffness devices, the proposed combined NSDO and CDO systems prove to be more effective with limited negative stiffness devices and thus provide more design flexibilities tailored to different application situations.

1. Introduction

The conventional outrigger (CO) systems that configure outriggers between the perimeter columns and the core have shown to be effective to reduce the overall lateral displacement of the building and the base bending moment of the core and thus ensure the safety of tall buildings under static lateral loads such as mean wind load [1, 2]. However, the majority of the external excitations that tall buildings encounter are dynamic loadings [3], and the CO systems are difficult to provide sufficient damping to suppress excessive vibration for high-rise structures [4–8]. Therefore, extra energy dissipation means are generally needed for tall buildings to improve the seismic safety.

Smith and Willford first proposed the novel concept of damped outrigger systems by introducing viscous dampers vertically between perimeter columns and the end of outriggers (referred to as conventional damped outrigger (CDO) systems hereafter, see Figure 1 [9]) and demonstrated the excellent control performance of such systems under wind loadings [9, 10]. Soon some researchers applied the CDO systems to improve the seismic performance of tall buildings [11–13]. Subsequently, the control performance of the damped outrigger systems was investigated subjected to multiple hazards, e.g.,

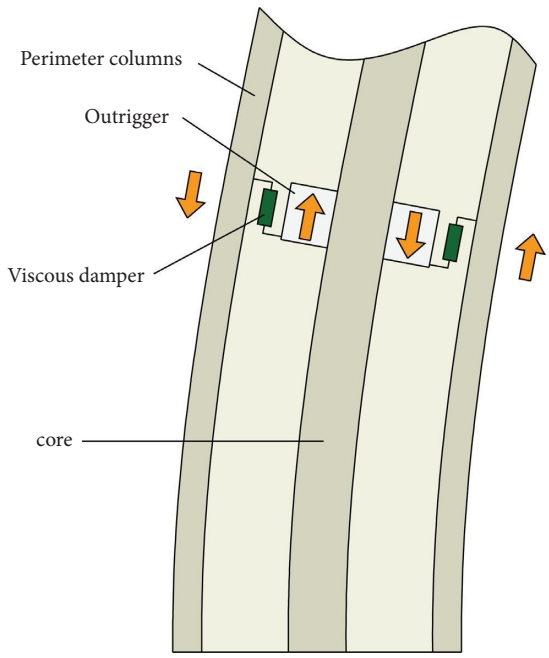

Figure 1: Conceptual details of the outrigger damper system.

earthquake and wind [14, 15]. These investigations have shown superior performance of the damped outrigger systems over the conventional outrigger systems by providing significant supplementary damping to the structures.

Because the CDO systems in essence are to fully utilize the large vertical relative deformation between outrigger ends and perimeter columns and provide additional damping for the whole structures, a good number of studies were aimed to achieve maximum supplementary damping and the associated with optimal design [16, 17].To achieve satisfactory modal damping ratios, however, the perimeter columns in the CDO systems were required to have adequate axial stiffness [18–20]. Such finding was consistent with previous result of the damping effect of Maxwell damping element (MDE) if the assembly of outrigger viscous damper and perimeter column was viewed as a MDE and the damping effect would be limited with insufficient MDE stiffness [21–23]. Further improvement of such systems on adding damping could be beneficial when increasing the size of perimeter columns might not be desirable.

To relax the restriction of perimeter column and improve the damping behavior of damped outrigger systems, one of the promising solutions is the introduction of negative stiffness devices which have proven to amplify the relative motion between their two terminals as with inerter dampers [24–28]. For instance, Shi and Zhu [29] conducted a comparative study of using negative stiffness damper and inerter damper for vibration isolation, while Li et al. [30] incorporated negative stiffness element with controllable damping element to achieve quasiactive control effect under earthquake. Wang et al. [31] proposed a negative stiffness damped outrigger (NSDO) system within which negative stiffness devices were incorporated in parallel with viscous dampers in the CDO system, and significant improvement on maximum damping ratio for structures with only one damped outrigger. Due to the interaction of outriggers, however, the NSDO systems with multiple damped outriggers might not always have the maximum damping level compared to the corresponding CDO systems (see [32] for more details). Yet the introduction of NSDO presented inspirational development for damped outrigger systems as damped outriggers could be applied for wider scenarios without the need of significantly increasing the size of perimeter columns.

While design based on maximum modal damping ratio generally produces acceptable control effect, such design could not guarantee optimal control results for stochastic excitations. By modeling the stochastic seismic excitation as filtered white noise, Fang et al. [33] proposed a stochastic optimization procedure and applied it to the design of the CDO systems with the seismic excitation modeled as Kanai–Tajimi spectrum. Sun et al. [34] further extended the above procedure to parametrically investigate the optimum parameters of the NSDO system where the Clough–Penzien (CP) model was used to model seismic excitation. These studies investigated the optimal designs of damped outrigger systems with the seismic excitation modeled as a stationary stochastic process. To date, engineering applications of damped outriggers in buildings can be found in [9, 35, 36], and an interesting application scenario is to mitigate vibration of long-span bridges [37].

Despite the advancement thus far, five main issues exist. First, as with modal damping analysis mentioned above, the structures with multiple NSDOs might not always be the optimal solution due to the interaction of outriggers, and further examination of the design and performance of multiple NSDO systems is necessary. Second, although the previous studies combined the CO either with the CDO [19] or with NSDO [15, 31, 34], the potential benefit of combining the CDO and NSDO has not been explored. Third, the stochastic analysis of damped outrigger systems considering the uncertainty of earthquake previously adopted the assumption of stationary, but the natural seismic excitations often exhibits nonstationary characteristics [38–40]; unless the analysis results obtained from stationary excitation assumption for such systems are formally justified, designing the outrigger systems and evaluating the performance subjected to nonstationary seismic excitation are more challenging and of great importance from practical perspective. Fourth, the parameters of installed devices obviously affect the system seismic performance, and this is particularly the case for the NSDO system where the negative stiffness devices play a significant role in structural dynamic characteristic, but the sensitivity on desired objectives has not been studied. Finally, to make the stochastic optimization more intuitive and align with engineering practice, the obtained optimal design needs to be further examined under both real far and near-field earthquake records.

This paper proposes a stochastic optimization method to investigate optimal configurations of combined negative stiffness damped outriggers (NSDOs) and conventional damped outriggers (CDOs) subjected to nonstationary stochastic seismic excitation. In this study, three types of damped outrigger systems considered are (1) the conventional viscously damped outrigger placed above the negative stiffness outrigger, referred to as C&N hereafter; (2) the NSDO placed above the CDO, referred to as N&C hereafter,

and (3) the double NSDOs, referred to as DN hereafter. First, the simplified analysis model of various combinations of damped outriggers is developed, and the state-space representation of outrigger systems is formulated. Second, the nonstationary seismic excitation is modeled as a uniformly modulated stationary Gaussian process with a time-modulating function following CP spectrum. Third, combining equations of motions of outrigger systems and seismic excitation gives rise to the augmented state-space representation of structure-damper-excitation and subsequently the differential Lyapunov equation. Fourth, the optimal designs of damped outriggers are defined via the solution of the differential Lyapunov equation, and the multiobjective optimization with Pareto optimal fronts is adopted to deal with conflicting objectives, followed by the sensitivity of negative stiffness ratio on design objectives. Finally, the efficacy of the proposed method is demonstrated through a tall building designed with various damped outriggers and the optimal designs are further examined under real earthquake records.

2. Problem Formulation

This section presents the stochastic analysis for the mixed NSDO and CDO systems subject to nonstationary seismic excitation. First, a simplified structural model of these outrigger systems is developed. With the motion equations of structure-damper-excitation, the state-space representation is formulated. The nonstationary seismic excitation is then modeled as uniformly modulated stationary Gaussian stochastic process, where the CP model is adopted to deal with low frequency issue. Finally, an augmented state-space representation of such systems with seismic excitation considered is formulated and subsequently the differential Lyapunov equation governing the stochastic structural responses is formulated, the root-mean-square (RMS) values of which will be used as optimization objectives.

2.1. Simplified Model of the NSDO Systems. Inspired by active controllers that exhibit negative slope of force-deformation relationship, negative stiffness dampers (NSDs) could be realized through variable orifice dampers [41], semiactive dampers via linear quadratic regulator [42], precompressed springs [43], static and moving magnets integrated with eddy current [44], snap-through effect of a prebuckled beam [45], and inverted friction pendulum sliding dampers [46]. A well-developed NSD using a precompressed spring and a pivot plate is adopted to connect both perimeter columns and outrigger ends (see [34] for more details).

Figure 2 shows the equivalent models of different outriggers. For the CDO, shown in Figure 2(a), the force at the outrigger end produced by the viscous damper is

$$F_{CDO} = c_d\left(\dot{u} - \dot{u}_c\right), \tag{1}$$

where u and u_c are the vertical displacements of the ends of the outrigger and the perimeter column relative to the ground, respectively, the overdot represents derivative with respect to time, and c_{d} is the damping coefficient.

In Figure 2(b), a negative stiffness device is incorporated in parallel with a viscous damper in the NSDO, and the force at the outrigger end generated by the NSDO is

$$F_{NSDO} = k_{\mathrm{NS}}\left(u - u_{\mathrm{c}}\right) + c_{\mathrm{d}}\left(\dot{u} - \dot{u}_{\mathrm{c}}\right), \tag{2}$$

where k_{NS} is the negative stiffness. Obviously, the CDO can be viewed as the special case of the NSDO when $k_{NS} = 0$.

The simplified structural model for the NSDO system is shown in Figure 3, where different outrigger systems can be obtained with adjustment of the design parameters. EI, m, and H, respectively, indicate flexural rigidity, the mass per unit length, and the height of the core, which is modeled as a uniform Bernoulli–Euler beam.

The outriggers are assumed to have infinite flexural rigidity with the span of $2r$. The axial stiffness of the perimeter column is E_cA_c. Outriggers are located at a height of $\alpha_1 H$, …, $\alpha_j H$, …, $\alpha_n H$ from the bottom of the building, respectively. For convenience, the following derivation considers the NSDO system with two damped outriggers and can be easily extended to tall buildings with any number of outriggers.

The equilibrium equation between the NSDO and the perimeter column at the first outrigger is

$$\begin{cases} F_{r1} = k_{NS1}\left(u_1 - u_{\mathrm{c1}}\right) + c_{d1}\left(\dot{u}_1 - \dot{u}_{c1}\right), \\ k_{NS1}\left(u_{c1} - u_1\right) + c_{d1}\left(\dot{u}_{c1} - \dot{u}_1\right) + k_{c1}u_{c1} - k_{c2}\left(u_{c2} - u_{c1}\right) = 0, \end{cases} \tag{3}$$

where u_1 is the vertical displacements of the first outrigger end; u_{c1} is the axial deformation of perimeter column below the first outrigger; k_{NS1} and c_{d1} are the negative stiffness and damping coefficient of the first NSDO, respectively; and the axial stiffness of perimeter columns split by outriggers is $k_{\mathrm{c1}} = E_{\mathrm{c}}A_{\mathrm{c}}/\alpha_1 H, k_{\mathrm{c2}} = E_{\mathrm{c}}A_{\mathrm{c}}/\left(\alpha_2 - \alpha_1\right)H$.

The equilibrium equation between the NSDO and the perimeter column at the second outrigger is

$$\begin{cases} F_{r2} = k_{NS2}\left(u_2 - u_{\mathrm{c2}}\right) + c_{d2}\left(\dot{u}_2 - \dot{u}_{\mathrm{c2}}\right), \\ k_{NS2}\left(u_{\mathrm{c2}} - u_2\right) + c_{d2}\left(\dot{u}_{\mathrm{c2}} - \dot{u}_2\right) + k_{\mathrm{c2}}\left(u_{\mathrm{c2}} - u_{\mathrm{c1}}\right) = 0, \end{cases} \tag{4}$$

where u_2 is the vertical displacements of the second outrigger end; u_{c2} is the axial deformation of perimeter column between the second and the first outriggers; and k_{NS2} and c_{d2} are the negative stiffness and damping coefficient of the second NSDO, respectively.

Combining equations (1)–(4) leads to

$$\mathbf{F}_r = \mathbf{K}_{NS}\left(\mathbf{u} - \mathbf{u}_{\mathrm{c}}\right) + \mathbf{C}_d\left(\dot{\mathbf{u}} - \dot{\mathbf{u}}_c\right) = \mathbf{K}_{\mathrm{c}}\mathbf{u}_c, \tag{5}$$

where $\mathbf{F}_r = \left\{F_{r1}(t), F_{r2}(t)\right\}^{\mathrm{T}}$, $\mathbf{u} = \left\{u_1, u_2\right\}^{\mathrm{T}}$, $\mathbf{u}_c = \left\{u_{c1}, u_{c2}\right\}^{T}$, and

$$\mathbf{K}_{NS} = \begin{bmatrix} k_{NS1} & \\ & k_{NS2} \end{bmatrix}, \quad \mathbf{C}_d = \begin{bmatrix} c_{d1} & \\ & c_{d2} \end{bmatrix}, \quad \mathbf{K}_{\mathrm{c}} = \begin{bmatrix} k_{c1} + k_{c2} & -k_{c2} \\ -k_{c2} & k_{c2} \end{bmatrix}. \tag{6}$$

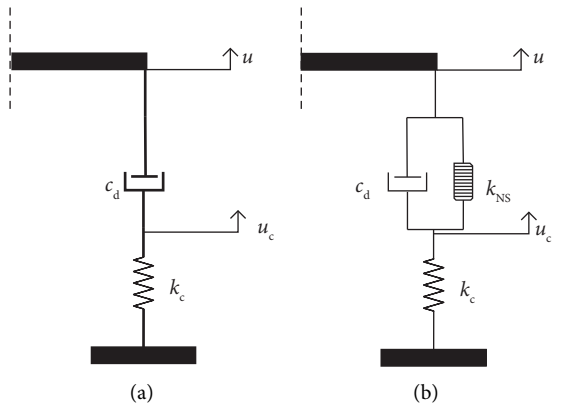

Figure 2: Equivalent model for (a) conventional damped outrigger (CDO) and (b) negative stiffness damped outrigger (NSDO).

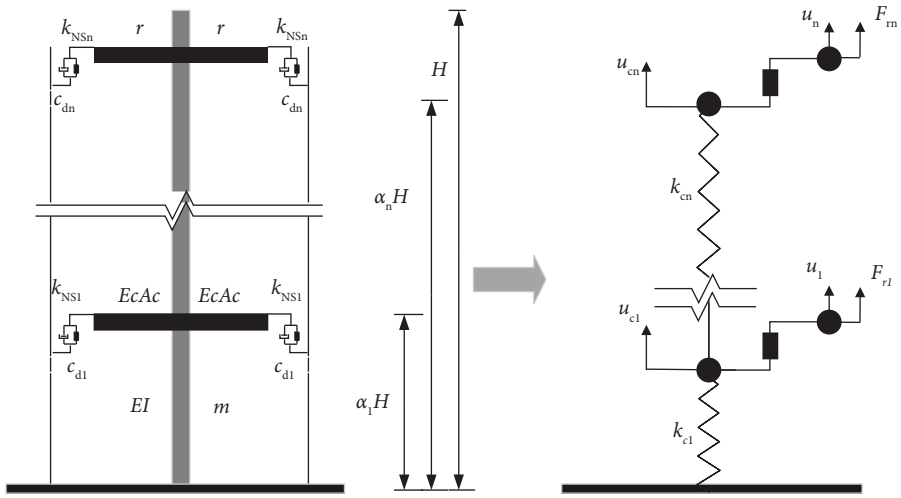

Figure 3: Simplified model of tall buildings with multiple NSDOs.

It should be pointed out that properly adjusting the parameters of viscous dampers and the negative stiffness in the NSDO systems results in various kinds of outrigger systems. For instance, the NSDO systems reduce to the CDO systems if all negative stiffness is set to zero and further reduce to either the CO systems with the viscous coefficient set to infinite or the bare structure (structure without outriggers, referred to as BS hereafter) if the viscous coefficient is set to zero. For multiple outrigger structures, the mixed NSDO and CO systems can be obtained when some of diagonal elements inthe negatives stiffness K_NS are set to zeros and some diagonal components in the viscous coefficient C_d infinite, while the mixed NSDO and CDO systems result from the diagonal entries of negative stiffness K_NS being partly set to zeros.

2.2. State-Space Representation of the NSDO. As in benchmark study, the tall building can be simplified as a cantilevered beam and the structural responses can be derived from it [47]. In this study, the finite element analysis method is used to derive the motion equation of the structural seismic response. The dynamic equation can be expressed as

$$\mathbf{M}\ddot{\mathbf{x}} + \mathbf{C}\dot{\mathbf{x}} + \mathbf{K}\mathbf{x} = \mathbf{F}_{\text{ext}} + \mathbf{F}_{\theta r}, \tag{7}$$

where $\mathbf{x} = [u_1, \theta_1, \cdots u_j, \theta_j \cdots u_n, \theta_n]^T$ is the displacement vector with u_j and θ_j representing the transverse and rotational components at the j-th story and n being the number of beam elements and **M**, **C**, and **K** are the global mass, damping, and stiffness matrices with **M** and **K** assembled from their corresponding element-wise mass and stiffness matrices modeled as a Bernoulli–Euler beam [48].

$$\mathbf{M}_e = \frac{mL_0}{420}\begin{bmatrix} 156 & 22L_0 & 54 & -13L_0 \\ 22L_0 & 4L_0^2 & 13L_0 & -3L_0^2 \\ 54 & 13L_0 & 156 & -22L_0 \\ -13L_0 & -3L_0^2 & -22L_0 & 4L_0^2 \end{bmatrix}, \tag{8}$$

where L_0 stands for the element length. Similarly, the stiffness matrix for one element is

$$\mathbf{K}_e = \frac{EI}{L_0^3}\begin{bmatrix} 12 & 6L_0 & -12 & 6L_0 \\ 6L_0 & 4L_0^2 & -6L_0 & 2L_0^2 \\ -12 & -6L_0 & 12 & -6L_0 \\ 6L_0 & 2L_0^2 & -6L_0 & 4L_0^2 \end{bmatrix}. \tag{9}$$

Also, the global damping matrix $\mathbf{C}$ can be constructed by Rayleigh assumption.

Substituting $u = r\theta_n = r\Gamma^T x$ into equation (7), $\mathbf{F}_{\theta r}$ can be expressed as

$$\mathbf{F}_{\theta r} = -2\mathbf{F}_r r = -2r\left(\mathbf{K}_{NS}\left(r\Gamma^T\mathbf{x} - \mathbf{u}_c\right) + \mathbf{C}_d\left(r\Gamma^T\dot{\mathbf{x}} - \dot{\mathbf{u}}_c\right)\right), \tag{10}$$

where Γ is the position vector of the outriggers. In addition, the inertial force caused by earthquake on one Bernoulli–Euler beam element is given by [49]

$$\mathbf{F}_{ej} = \frac{-m\ddot{x}_g L_0}{12}\begin{bmatrix} 6 & L_0 & 6 & -L_0 \end{bmatrix}, \tag{11}$$

where $\ddot{x}_g$ is the acceleration of horizontal ground motion and $L_0 = H/n$ is the length of the discretized element.

The seismic excitation $\mathbf{F}_{\text{ext}}$ can be formulated as

$$\mathbf{F}_{\text{ext}} = \boldsymbol{\delta}\ddot{x}_g, \tag{12}$$

where δ is the earthquake action vector assembled from $\mathbf{F}_{ej}$.

In this study, three parameters design variables considered: dimensionless negative stiffness ratio η, dimensionless outrigger damping coefficient c, and outrigger location N_0. Also, the dimensionless parameters c, β, and η are defined as [34]

$$c = \frac{c_d r^2}{H\sqrt{mEI}}, \beta = \frac{EI}{2E_c A_c r^2}, \eta = \frac{k_{NS}Hr^2}{EI}. \tag{13}$$

Substituting equations (10)–(13) into equation (7) yields the following equation:

$$\mathbf{M}_r\ddot{\mathbf{x}}_r + \mathbf{C}_r\dot{\mathbf{x}}_r + \mathbf{K}_r\mathbf{x}_r = \mathbf{P}_r, \tag{14}$$

with $\mathbf{M}_r$, $\mathbf{C}_r$, $\mathbf{K}_r$, and $\mathbf{x}_r$ as follows:

$$\mathbf{M}_r = \begin{bmatrix} \mathbf{M} & 0 \\ 0 & \mathbf{m}_e \end{bmatrix}, \mathbf{C}_r = \begin{bmatrix} \mathbf{C} + \Gamma 2\mathbf{C}_d r^2\Gamma^T & -2\mathbf{C}_d r\Gamma \\ \mathbf{C}_d r\Gamma^T & -\mathbf{C}_d \end{bmatrix}, \tag{15a}$$

$$K_r = \begin{bmatrix} \mathbf{K} + \Gamma 2\mathbf{K}_{NS} r^2\Gamma^T & -2\mathbf{K}_{NS} r\Gamma \\ \mathbf{K}_{NS} r\Gamma^T & -\left(\mathbf{K}_c + \mathbf{K}_{NS}\right) \end{bmatrix}, \mathbf{x}_r = \begin{pmatrix} \mathbf{x} \\ u_c \end{pmatrix}, \mathbf{P}_r = \begin{pmatrix} \mathbf{F}_{\text{ext}} \\ 0 \end{pmatrix}, \tag{15b}$$

where $\mathbf{m}_e$ is the virtual mass of the connection between the perimeter column and the damper, and its value is set very small to avoid the singularity of the mass matrix $\mathbf{M}_r$ [50].

$$C_d = \begin{bmatrix} \frac{c_1 H\sqrt{mEI}}{r^2} & \\ & \frac{c_2 H\sqrt{mEI}}{r^2} \end{bmatrix}, K_{NS} = \begin{bmatrix} \frac{EI\eta_1}{Hr^2} & \\ & \frac{EI\eta_2}{Hr^2} \end{bmatrix}, K_c = \begin{bmatrix} \frac{EI}{2r^2\beta\alpha_1 H} + \frac{EI}{2r^2\beta(\alpha_2-\alpha_1)H} & -\frac{EI}{2r^2\beta(\alpha_2-\alpha_1)H} \\ -\frac{EI}{2r^2\beta(\alpha_2-\alpha_1)H} & \frac{EI}{2r^2\beta(\alpha_2-\alpha_1)H} \end{bmatrix}. \tag{16}$$

From equation (14), the state-space representation of the NSDO systems can be expressed as

$$\begin{aligned} \dot{\mathbf{Z}}_r &= \mathbf{A}_b\mathbf{Z}_r + \mathbf{B}_b, \\ \mathbf{Y}_r &= \mathbf{C}_b\mathbf{Z}_r + \mathbf{D}_b, \end{aligned} \tag{17}$$

where $\mathbf{Z}_r = \begin{pmatrix} \mathbf{x}_r \\ \dot{\mathbf{x}}_r \end{pmatrix}, \mathbf{A}_b = \begin{pmatrix} \mathbf{0} & \mathbf{I} \\ -\mathbf{M}_r^{-1}\mathbf{K}_r & -\mathbf{M}_r^{-1}\mathbf{C}_r \end{pmatrix}, B_b = \begin{pmatrix} \mathbf{0} \\ \mathbf{M}_r^{-1}\mathbf{P}_r \end{pmatrix}$, and $\mathbf{C}_b$ and $\mathbf{D}_b$ are output matrices determined by output variable $\mathbf{Y}_r$. If the displacement and acceleration are selected to form the output vector, we will have the following expression:

$$\mathbf{C}_b = \begin{bmatrix} \mathbf{I} & \mathbf{0} \\ -\mathbf{M}_r^{-1}\mathbf{K}_r & -\mathbf{M}_r^{-1}\mathbf{C}_r \end{bmatrix}, \mathbf{D}_b = \begin{bmatrix} \mathbf{0} \\ \mathbf{M}_r^{-1}\mathbf{P}_r \end{bmatrix}. \tag{18}$$

2.3. Nonstationary Stochastic Seismic Excitation. Assuming that the evolution of the frequency content with time can be neglected, the earthquake excitation is considered as a uniformly modulated stationary Gaussian stochastic process with a zero mean described by the two-

side evolutionary power spectral density (PSD) function, that is [51],

$$S_{\ddot{x}_g}(\omega) = |\phi(t)|^2 S_{\ddot{x}_f}(\omega), \tag{19}$$

where $\phi(t)$ is the time-modulating function expressed as

$$\phi(t) = \begin{cases} \left(\dfrac{t}{t_1}\right)^{\alpha} (0 \le t \le t_1), \\ 1\,(t_1 \le t \le t_2), \\ e^{-(t-t_2)/\tau}\,(t_2 \le t \le T_D), \end{cases} \tag{20}$$

where t_1 and t_2 are the start and end time of the strong motion duration, respectively; α and τ are the constant shape coefficients; and T_D is the strong motion duration. The envelope function is shown in Figure 4.

The Clough–Penzien (CP) model is introduced to correct the unrealistically high values of the power spectral density function at low frequency in the Kanai–Tajimi spectrum [52].

$$S_{\ddot{x}_f}(\omega) = S_0 \left(\frac{\omega_g^4 + 4\xi_g^2\omega_g^2\omega^2}{\left(\omega_g^2 - \omega^2\right)^2 + 4\xi_g^2\omega_g^2\omega^2}\right)\left(\frac{\omega^4}{\left(\omega_f^2 - \omega^2\right)^2 + 4\xi_f^2\omega_f^2\omega^2}\right), \tag{21}$$

where S_0 is the two-sided power spectral density of the input white noise, ω_g and ξ_g are the site predominant frequency and damping ratio for the high-frequency constant, respectively, and ω_f and ξ_f are the corresponding parameters for the low-frequency constant, respectively.

Thus, the earthquake acceleration $\ddot{x}_g(t)$ is expressed as

$$\ddot{x}_g(t) = \phi(t)\ddot{x}_f(t), \tag{22}$$

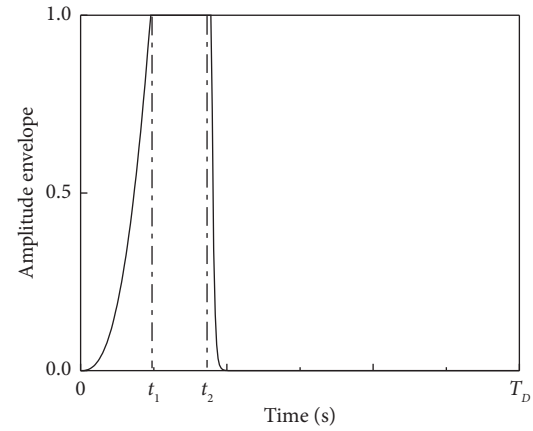

Figure 4: Nonstationary amplitude envelope function.

where $\ddot{x}_f(t)$ is a stochastic stationary process and can be considered as the response of two linear filters subject to white-noise excitation w with a constant PSD as follows:

$$\ddot{x}_f(t) + 2\xi_f\omega_f\dot{x}_f(t) + \omega_f^2 x_f(t) = -\ddot{x}_0(t) - w(t), \tag{23}$$

$$\ddot{x}_0(t) + 2\xi_g\omega_g\dot{x}_0(t) + \omega_g^2 x_0(t) = -w(t), \tag{24}$$

where $x_0(t)$ is the response of the first filter.

Defining $\mathbf{Z}_g = \begin{bmatrix} x_f & x_0 & \dot{x}_f & \dot{x}_0 \end{bmatrix}^T$, equations (23) and (24) can be then expressed in the state-space form as

$$\begin{aligned} \dot{\mathbf{Z}}_g &= \mathbf{A}_g\mathbf{Z}_g + \mathbf{B}_g w(t), \\ \ddot{x}_g(t) &= \mathbf{C}_g\mathbf{Z}_g, \end{aligned} \tag{25}$$

where $\mathbf{A}_g$, $\mathbf{B}_g$, and $\mathbf{C}_g$ represent the characteristics of the excitation, which are given by

$$\mathbf{A}_g = \begin{bmatrix} 0 & 0 & 1 & 0 \\ 0 & 0 & 0 & 1 \\ -\omega_f^2 & \omega_g^2 & -2\xi_f\omega_f & 2\xi_g\omega_g \\ 0 & -\omega_g^2 & 0 & -2\xi_g\omega_g \end{bmatrix}, \quad \mathbf{B}_g = \begin{bmatrix} 0 \\ 0 \\ 0 \\ -1 \end{bmatrix}, \quad \mathbf{C}_g = \phi(t)\begin{bmatrix} -\omega_f^2 & \omega_g^2 & -2\xi_f\omega_f & 2\xi_g\omega_g \end{bmatrix}. \tag{26}$$

2.4. RMS Values of Structural Response. An augmented state vector, $\mathbf{Z}_a$, is defined as $\mathbf{Z}_a = \begin{bmatrix} \mathbf{Z}_r^T & \mathbf{Z}_g^T \end{bmatrix}^T$ to yield a combined representation of a controlled structure and excitation:

$$\begin{aligned} \dot{\mathbf{Z}}_a &= \mathbf{A}_a\mathbf{Z}_a + \mathbf{B}_a w(t), \\ \mathbf{y}_a &= \mathbf{C}_a\mathbf{Z}_a, \end{aligned} \tag{27}$$

$$\mathbf{A}_a = \begin{bmatrix} \mathbf{A} & \mathbf{B}\mathbf{C}_g \\ \mathbf{0} & A_g \end{bmatrix}, \mathbf{B}_a = \begin{bmatrix} \mathbf{0} \\ \mathbf{B}_g \end{bmatrix}, \mathbf{C}_a = \begin{bmatrix} \mathbf{C} & \mathbf{D}\mathbf{C}_g \end{bmatrix}.$$

The covariance of the structural responses is employed to assess structural performance. The covariance matrix $\Gamma_{X_a} = E[(\mathbf{x}_a - \mu_{x_a})(\mathbf{x}_a - \mu_{x_a})^T]$ of the vector $\mathbf{Z}_a$ is determined through the solution of

$$\dot{\Gamma}_{x_a} = \mathbf{A}_a\Gamma_{x_a} + \Gamma_{x_a}\mathbf{A}_a^T + 2\pi B_a\mathbf{S}_0\mathbf{B}_a^T. \tag{28}$$

Assuming that the initial conditions are deterministic, $\Gamma_{x_a}(0) = \Gamma_0 = 0$, to solve equation (28). $\dot{\Gamma}_{x_a}$ at a given time (t) is described using a backward difference scheme [51]:

$$\dot{\Gamma}_{x_a}(t) = \frac{\Gamma_{x_a}(t) - \Gamma_{x_a}(t-1)}{\Delta t}, \tag{29}$$

where Δt is the time interval.

At each time interval, structural responses are obtained using the solution of

$$(\Delta t\mathbf{A}_a - \mathbf{I})\Gamma_{x_a}(t) + \Delta t\Gamma_{x_a}(t)\mathbf{A}_a^T + \left[2\pi\Delta t\mathbf{B}_a\mathbf{S}_0\mathbf{B}_a^T + \Gamma_{x_a}(t-1)\right] = \mathbf{0}. \tag{30}$$

In the case of $\phi(t) = 1$, as $\Delta t \longrightarrow \infty$, the seismic loading became a stationary stochastic process. The stationary solution can be obtained directly as a solution of the Lyapunov equation:

$$\dot{\Gamma}_{x_a} = \mathbf{A}_{\mathrm{a}}\Gamma_{x_a} + \Gamma_{x_a}\mathbf{A}_a^T + 2\pi\mathbf{B}_{\mathrm{a}}\mathbf{S}_0\mathbf{B}_a^T = \mathbf{0}. \tag{31}$$

Finally, the RMS response of the output structural responses is given by

$$\left\|Y_a\right\|_{RMS} = \sqrt{\mathrm{diag}\left(\mathbf{C}_a\Gamma_{x_a}\mathbf{C}_a^T\right)}, \tag{32}$$

where diag $(\cdot)$ is the diagonal term of a square matrix.

3. Multiobjective Optimization

In engineering practice, the specific design of a building at hand is supposed to meet various kinds of requirements with limited available resources, and how to achieve the goal while minimizing the use of resources is challenging. In this section, two main objectives associated with the safety and serviceability of tall buildings, harmful interstory drift and floor acceleration, are first defined and the definition of the former is briefly introduced. The Pareto optimal front is then used to provide trade-off between conflicting objectives. Finally, a procedure to implement multiobjective optimization approach is outlined.

3.1. Structural Optimization Formulation. The optimization problem can be defined as follows:

$$\begin{aligned} &\text{design variables: } v = \{\eta \quad c \quad N_0\}^{\mathrm{T}} \\ &\text{minimize: } J_{\mathrm{dual}}(v) \\ &\text{subject to: } \begin{cases} G(Y_{\mathrm{a}}, v) \le 0 \\ v_{\min} \le v \le v_{\max} \end{cases} \end{aligned}, \tag{33}$$

where v is the design variable, J_{dual} indicates the objective function related to harmful interstory drift and floor absolute acceleration, $G(Y_{\mathrm{a}}, v)$ is defined as the constrained function of design variables and responses, which could be empty if not specified explicitly, and $v_{\min}$ and $v_{\max}$ are the lower and upper bounds of design variables, respectively.

3.2. Optimization Objectives. Because different objectives might have several orders of difference in magnitude and cause numerical issues during calculation, the two objectives used herein are defined as the maximum structural responses of the damped outrigger systems normalized by the corresponding responses of the bare structure (BS), which are given as

$$J_{\mathrm{hdr}} = \frac{\max(T_{\mathrm{hdr}})}{\max(T_{\mathrm{hdr0}})}, \tag{34}$$

$$J_{\mathrm{acc}} = \frac{\max(T_{\mathrm{acc}})}{\max(T_{\mathrm{acc0}})}, \tag{35}$$

where T_{hdr} and T_{acc} are the RMS values of the harmful interstory drift ratio and floor absolute acceleration of the damped outrigger systems under nonstationary stochastic excitation obtained from equation (32), respectively, whereas the subscript "0" indicates the corresponding response quantity of the BS, and $\max(\cdot)$ denotes the maximum value inside the bracket. The harmful interstory drift ratio in equation (34) will be briefly revisited below.

Traditionally, the interstory drift ratio θ_i of the i-th story has been adopted as a performance index and can be expressed as [53]

$$\theta_i = \frac{\Delta u_i}{h_i}, \tag{36}$$

where Δu_i is interstory drift of the i-th story, respectively, and h_i the height of the i-th story.

Examination of the interstory drift in equation (36), however, reveals that the total drift consists of three components: interstory shear drift Δu_{si}, bending-induced flexural drift Δu_{bi}, and drift Δu_{ri} due to rigid body rotation of the floor, as shown in Figure 5 [54]. While the first two components could cause damage to the structures and hence the name harmful interstory drift, the last one is considered harmless to the related story. Recently, researchers argued that the harmless drift should be removed and the focus should be placed on harmful interstory drift for design purpose [33]. As such, the harmful interstory drift is adopted as the seismic performance index and can be calculated by the secant method [54]:

$$\widetilde{\theta}_i = \frac{\Delta u_i}{h_i} - \frac{\Delta u_{i-1}}{h_{i-1}} = \theta_i - \theta_{i-1}. \tag{37}$$

3.3. Pareto Optimal Fronts. For multiobjective optimization, the ideal situation is to optimize all the objectives simultaneously, which is typically not the case in the real world; some objectives are conflicting, i.e., minimization of one objective leads to amplification of other objectives. Such problem can be solved by using Pareto optimal fronts, which associate each objective a weight to reflect the trade-off between conflicting objectives and transform the multiobjective optimization into single objective design. In particular, the Pareto optimal front J_{dual} balancing the objectives of harmful interstory drift and floor acceleration is defined as [34]

$$J_{\mathrm{dual}} = \zeta J_{\mathrm{acc}} + (1-\zeta)J_{\mathrm{hdr}}, \tag{38}$$

where $\zeta \in [0, 1]$ is the weight value for the dual-response design function. When $\zeta = 1$, $J_{\mathrm{dual}} = J_{\mathrm{acc}}$, which represents

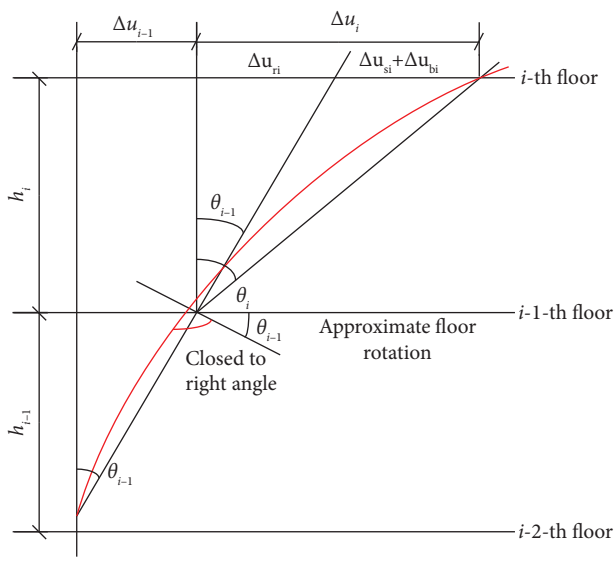

Figure 5: Illustration of interstory drift components.

the optimization based on harmful interstory drift, whereas $\zeta = 0, J_{\text{dual}} = J_{\text{hdr}}$, which refers to the optimization based on floor acceleration.

The steps to implement the multiobjective optimization method proposed in this paper are shown in the flowchart in Figure 6. During optimization, the generalized pattern search (GPS) algorithm is adopted because of its capability of dealing with noncontinuous and nondifferentiable objective functions [55, 56], which is available with the functions "patternsearch" and "fminsearch" in MATLAB toolbox.

4. An Illustrated Example

This section demonstrates the stochastic optimization approach with an illustrated example. This section starts with a description of tall building with two damped outriggers in the forms of C&N, N&C, and DN. Stochastic optimization of three damped outrigger systems based on single objective subjected to stationary and nonstationary seismic excitation is compared. As the objectives are conflicting, the Pareto optimal fronts are used to provide trade-off, and sensitivity of negative stiffness ratio on design objectives is investigated.

4.1. Building Information. The numerical example used herein to demonstrate the stochastic optimization procedure is a 60-story building. The main model parameters are as follows: the height of the building $H = 200\,m$, the flexural rigidity of the core $EI = 1.47 \times 10^{13}\,\text{Nm}^2$, distributed mass along the height of the core $m = 1.08 \times 10^5\,\text{kg/m}$, and the span of outrigger $r = 15\,\text{m}$. The dimensionless stiffness ratio of core to perimeter column $\beta = 2$ [48]. The first three natural frequencies of the bare structure (structure without outriggers, BS) are 0.1632 Hz, 1.0228 Hz, and 2.8940 Hz. As shown in Figure 3, the two damped outriggers are designed as the mixed CDO and NSDO, i.e., either the CDO over the NSDO (C&N) or the NSDO over CDO (N&C), and double NSDOs (DN), where outriggers are assumed to have infinite flexural rigidity as described in Section 2.1. The finite element method is used to analyze the damped outrigger systems, and the building is divided into 60 elements with each story consisting a beam element; the damping matrix **C** is constructed by Rayleigh assumption, and the damping ratio of the first and third modes is assumed as 0.02.

In the random seismic response analysis, the selected parameters of CP spectrum model are $S_0 = 4.62 \times 10^{-4}\,\text{m}^2/\text{s}^3$, $\omega_g = 15$ rad/s, $\xi_g = 0.6$, $\omega_f = 1.5$ rad/s, and $\xi_f = 0.6$. These parameters are selected from [57] to reflect firm-soil conditions. The parameters for the nonstationary envelope function given in equation (20) are taken to be $t_1 = 4.78\,s$, $t_2 = 8.96\,s$, $\alpha = 2.60$, and $\tau = 0.13$; the earthquake duration is chosen as $T_D = 30\,s$ [52]. During the process of optimization, the upper level of damped outriggers is fixed at the top as the conventional configuration in the outrigger systems, and the elevation of the lower outrigger is considered as design variable. Meanwhile, the dimensionless viscous coefficient is within the range of [0, 1], and the dimensionless negative stiffness coefficient η is set within the range of [−0.1, 0] because too small value of it will cause instability of system [31]. During analysis, the main structure is assumed to remain linear.

4.2. Single-Objective Optimization. Before getting into the insight of the damped outrigger systems, the nonstationary and stationary response envelopes of the harmful interstory drift and floor absolute acceleration of the BS as well as the corresponding maximum values evolving with time are shown in Figure 7. As observed in Figure 8, the peak RMS structural responses under nonstationary stochastic excitation occur after the strong motion duration ends. Moreover, the stationary responses of the BS overestimate the responses by 15.62% in maximum harmful interstory drift ratio and 16.52% in maximum floor absolute acceleration, i.e., the stationary optimization might lead to over-conservative results. This is mainly because the time-modulating function $\varphi(t)$ of the stationary stochastic excitation is 1 (see equation (20)). Furthermore, while the structural maximum acceleration occurs at the top, the maximum harmful interstory drift ratio of structure appears at the base, as opposed to the commonly used interstory drift ratio, which typically shows up at the upper levels in the tall buildings.

With the proposed stochastic optimization, the optimal results of different outrigger systems are listed in Table 1, and the response envelopes of different outrigger systems based on different objectives under nonstationary stochastic excitation are compared in Figures 8(a) and 8(b). Also shown in Figures 8(c) and 8(d) are the comparisons of the RMS values of the maximum harmful drift ratio and floor absolute acceleration under both kinds of excitations, which appear on the bottom and roof levels, respectively, where the responses of the structure under stationary stochastic excitation in dash lines are denoted by "(s)." As with the case of BS, the peaks of the RMS response under the nonstationary excitation occur after the strong motion duration, with the RMS stationary responses values of up to 6.82% and 9.24% overestimation on harmful interstory drift and floor acceleration, respectively. From Table 1, it can be observed that

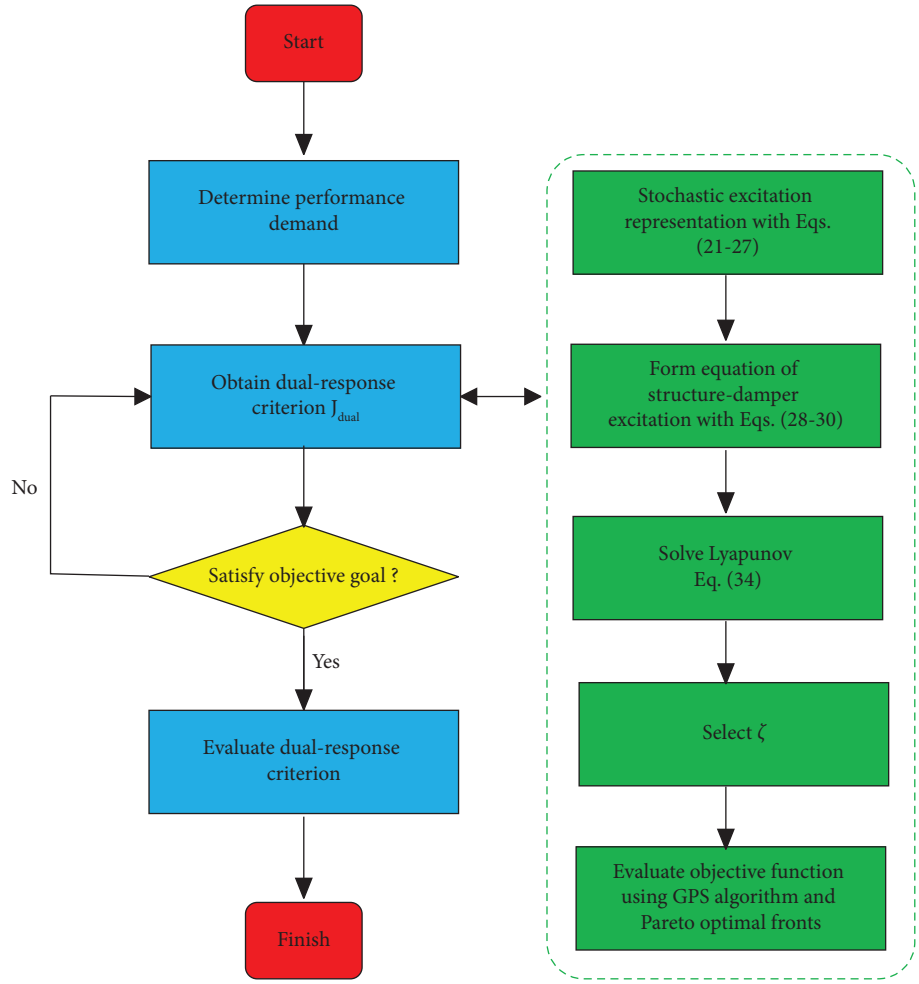

Figure 6: Dual-response design flowchart.

compared to the BS structure, all three damped outrigger systems have significant response reduction; specifically, around 36%–50% reduction in harmful interstory drift ratio and above 30% reduction in floor acceleration can be achieved when such systems are optimized based on harmful drift and floor acceleration, respectively. Among three damped outrigger systems, the DN system performs the best, while the C&N system has the compatible performance with the N&C system, and the latter performs slightly better than the former. Also observed is that these two objectives are conflicting. Take the N&C system as an example, and the optimal normalized harmful interstory drift ratio is 0.5966, but with acceleration as objective, it increases to 0.6169; likewise, the optimal normalized floor acceleration is 0.6658, but it becomes 0.6809 when using harmful drift as optimization objective. To deal with the competing objectives, the Pareto optimal fronts are adopted as a multiobjective optimization method to balance the two performance objectives and will be elaborated in the next section.

4.3. Multiobjective Optimization. As stated in the Section 3.2, the common solution for multiobjective optimization with conflicting objectives is to assign each objective a weight representing its importance, and Pareto optimal fronts provide design flexibility with changing weights of objectives.

To deal with the conflicting objectives and investigate the influence of stationarity of seismic excitation, Figures 9–11(a) show the Pareto optimal fronts of different outrigger systems subjected to nonstationary and stationary seismic excitation and Figures 9(b)–11(d) the associated with optimal designs. The optimal designs based on stationary excitation assumption are also evaluated under the condition of nonstationary seismic excitation and the results are also plotted in Figures 9–11(a). In Figures 9–11, "Opt-NS" and "Opt-S" indicate structural optimizations under nonstationary and stationary random excitations, respectively, while "Opt-S-NS" indicates that the stationary-based optimal design is evaluated under the condition of nonstationary seismic excitation.

In the case of the DN system, as observed in the Figure 11, the optimal damped outrigger locations coincide except for the weight being one with only one-story difference, and the maximum discrepancies of viscous coefficient and negative stiffness are 1.3% and 0.2%, respectively. Such tiny differences in the optimal design parameters have little influence for structures subjected to

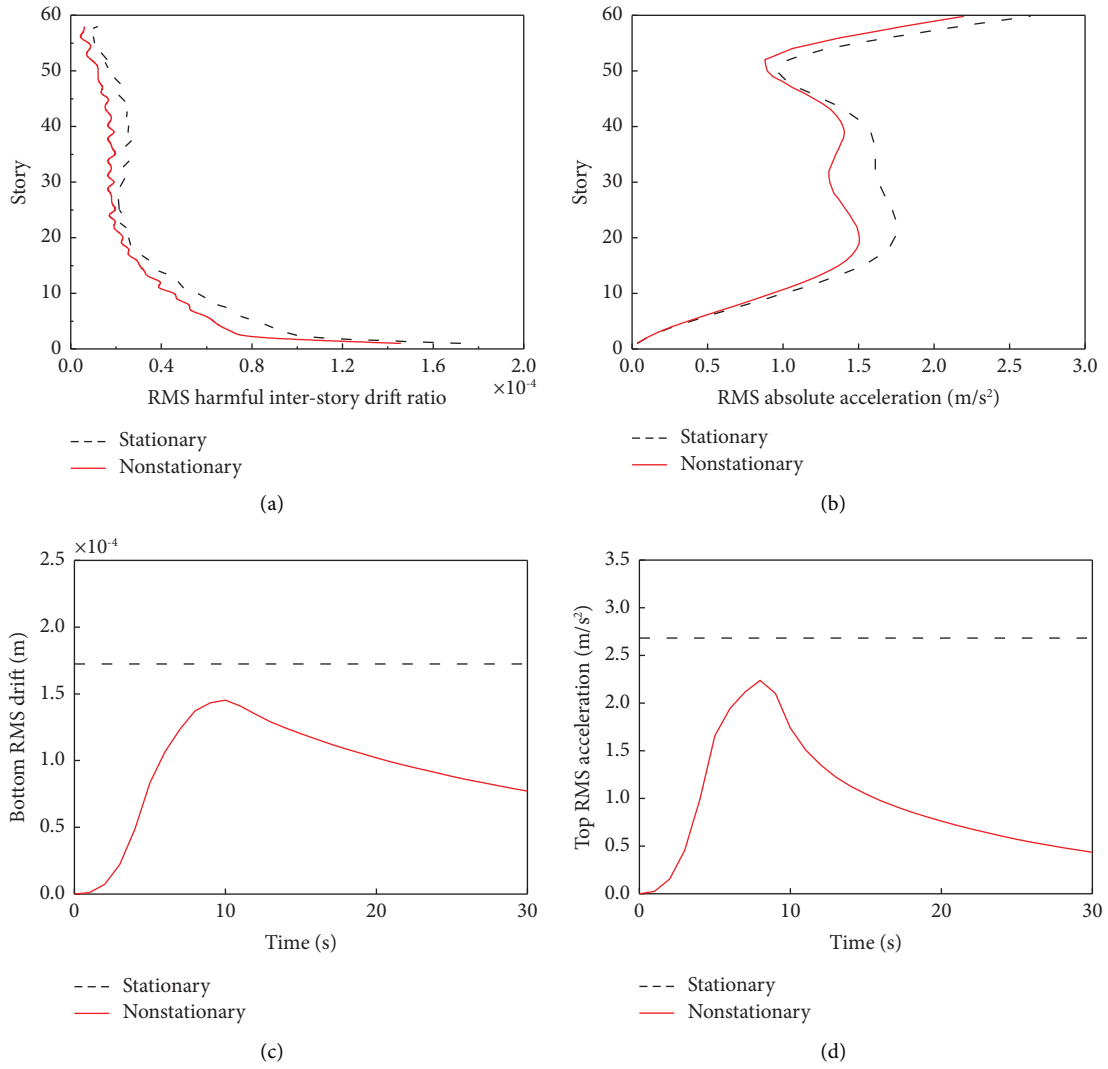

FIGURE 7: RMS response values of BS under nonstationary and stationary stochastic excitation. (a) Envelope of RMS harmful interstory drift ratio. (b) Envelope of RMS peak acceleration. (c) Bottom RMS harmful drift responses under both excitations. (d) Top RMS acceleration responses under both excitations.

nonstationary earthquake, i.e., the optimization using stationary assumption is justified. As for both cases of combining conventional damped outrigger and negative stiffness damped outrigger in Figures 9 and 10, the optimal elevations of damped outrigger have the maximum two-story distiction, and the optimal viscous coefficient and negative stiffness obtained from stationary excitation have 1.4% and 1.8% discrepancies compared to those obtained from nonstationary excitation. Moreover, these minor differences in optimal designs only have 1.2% performance deterioration and generally is considered negligible when damped outrigger systems are subjected to more realistic nonstationary seismic excitation. These investigations justify the use of stationary seismic excitation for damped outrigger systems during optimization, i.e., the less time-consumingstationary-based seismic optimization is adequate for engineering design practice, which is consistent with the findings for traditional buildings in [58]. For the sake of scrutiny, nonstationary-based optimization is still adopted in the following unless specified explicitly.

To see how the different configurations of damped outrigger systems behave, Figure 12 shows the Pareto optimal fronts of three outrigger systems under stationary and nonstationary seismic excitations, respectively. Apparently, the DN system performs the best in reducing both harmful interstory drift and structural acceleration, followed by the combined system with the negative stiffness outrigger placing over viscous damper outrigger. In other words, the DN system could have the best performance among the three damped outrigger systems with sufficient negative stiffness devices available.

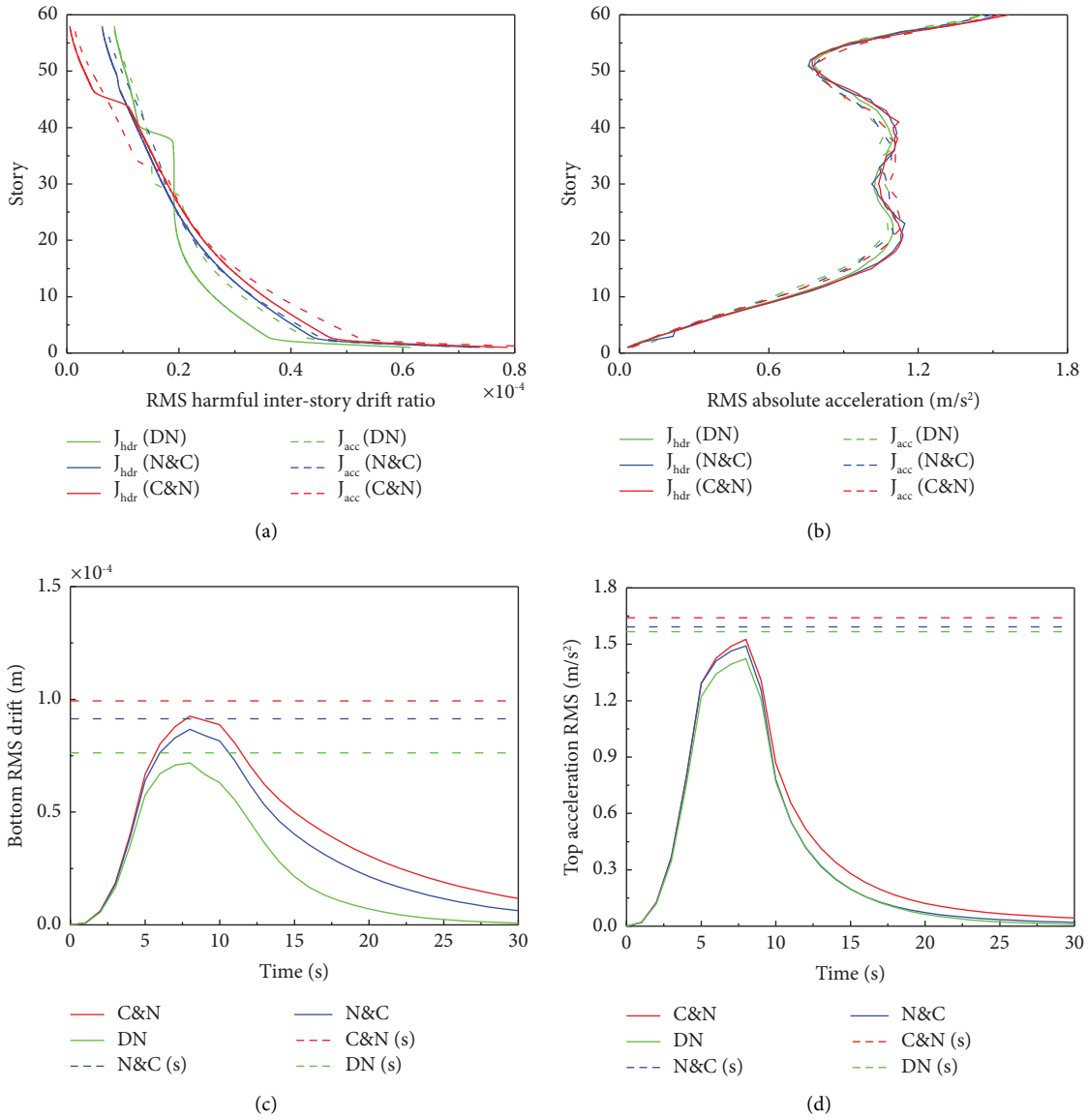

FIGURE 8: Comparisons of RMS response values of different outrigger systems. (a) RMS harmful interstory drift ratio under nonstationary excitation. (b) RMS peak acceleration under nonstationary excitation. (c) Bottom RMS drift under nonstationary and stationary stochastic excitation based on harmful interstory drift optimization. (d) Top RMS acceleration under nonstationary and stationary stochastic excitation based on floor acceleration optimization.

4.4. Sensitivity Analysis of Negative Stiffness Ratio. However, the above comparison is not completely fair because the DN system is using almost as twice amount of the negative stiffness devices as the N&C and C&N systems, and the optimal negative stiffness ratios for three systems in Figures 9–11(d)are close to the maximum allowable amount.Such suggest that the performance of three damped outrigger systems might be dominated by the amount of negative stiffness devices. Therefore, the sensitivity of system performance with respect to the total amount of negative stiffness ratio needs to be investigated and could be casted as constrained optimizations.

Figure 13 shows the Pareto optimal fronts of three damped outrigger systems with the maximum negative stiffness ratio varying from 0.05 to 0.1, and 0.13 only for the DN system. In Figure 13, the number inside the parentheses indicates the maximum total amount of negative stiffness ratio, e.g., "DN (0.05)" represents that Pareto front for the total normalized negative stiffness ratio ($-\eta$) in the range of 0–0.05. Comparing Figure 13 with Figures 9–12 shows that as the total amount of negative stiffness ratio available decreases (0.2 for the DN system and 0.1 for the other two), the systems decrease the reduction of the maximum harmful drift and floor absolute acceleration. More importantly, with the same total 0.5 negative stiffness ratio available, the C&N and N&C systems are superior to the DN system in reducing the harmful interstory drift and acceleration. When the maximum amount of negative stiffness ratio is 0.1, while the DN system performs slightly better than the C&N system, the N&C system still

Table 1: Detailed parameters and optimal results.

Objective	Parameter	C&N	N&C	DN
Harmful interstory drift ratio	η	−0.09977	−0.09902	−0.09387
	c	0.00984	0.00999	0.00791
	N_0	46	49	40
	J_{hdr}	0.6368	0.5966	0.4958
	J_{acc}	0.6977	0.6809	0.6497
Peak acceleration	η	−0.09858	−0.09899	−0.09378
	c	0.00985	0.00998	0.00787
	N_0	34	32	30
	J_{hdr}	0.7117	0.6169	0.5837
	J_{acc}	0.6815	0.6658	0.6355

C&N represents the conventional damped outrigger (CDO) placed above the negative stiffness damped outrigger (NSDO), while N&C represents the NSDO placed above the CDO, and DN denotes double NSDOs. Also, J_{hdr} and J_{acc} represent the objective values of harmful interstory drift ratio and floor absolute acceleration of damped outrigger systems based on the objectives specified in the first column, respectively.

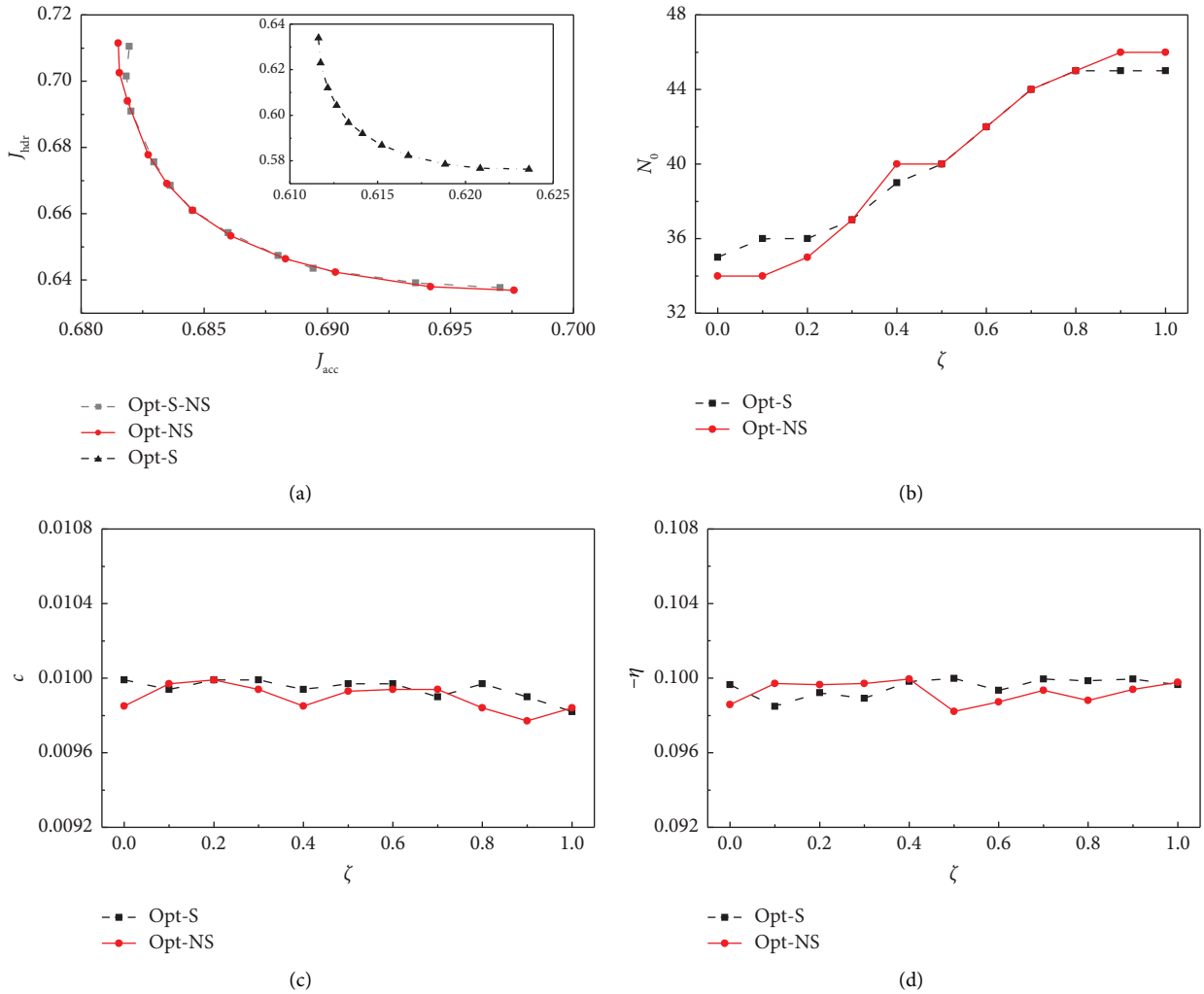

Figure 9: Optimal results for C&N. (a) Pareto front of performance indexes. (b) Optimal outrigger position. (c) Optimal outrigger damping coefficient. (d) Optimal negative stiffness ratio.

outperforms the other two and is still competitive against the DN system with $-\eta = 0.13$, where the former is slightly better than the latter on the right side of the intersection and less appealing on the left.

To see more clearly the sensitivity of negative stiffness ratio on the seismic performance, consider the three damped outrigger systems with the design objectives of balancing the mitigation on harmful interstory drift and floor acceleration

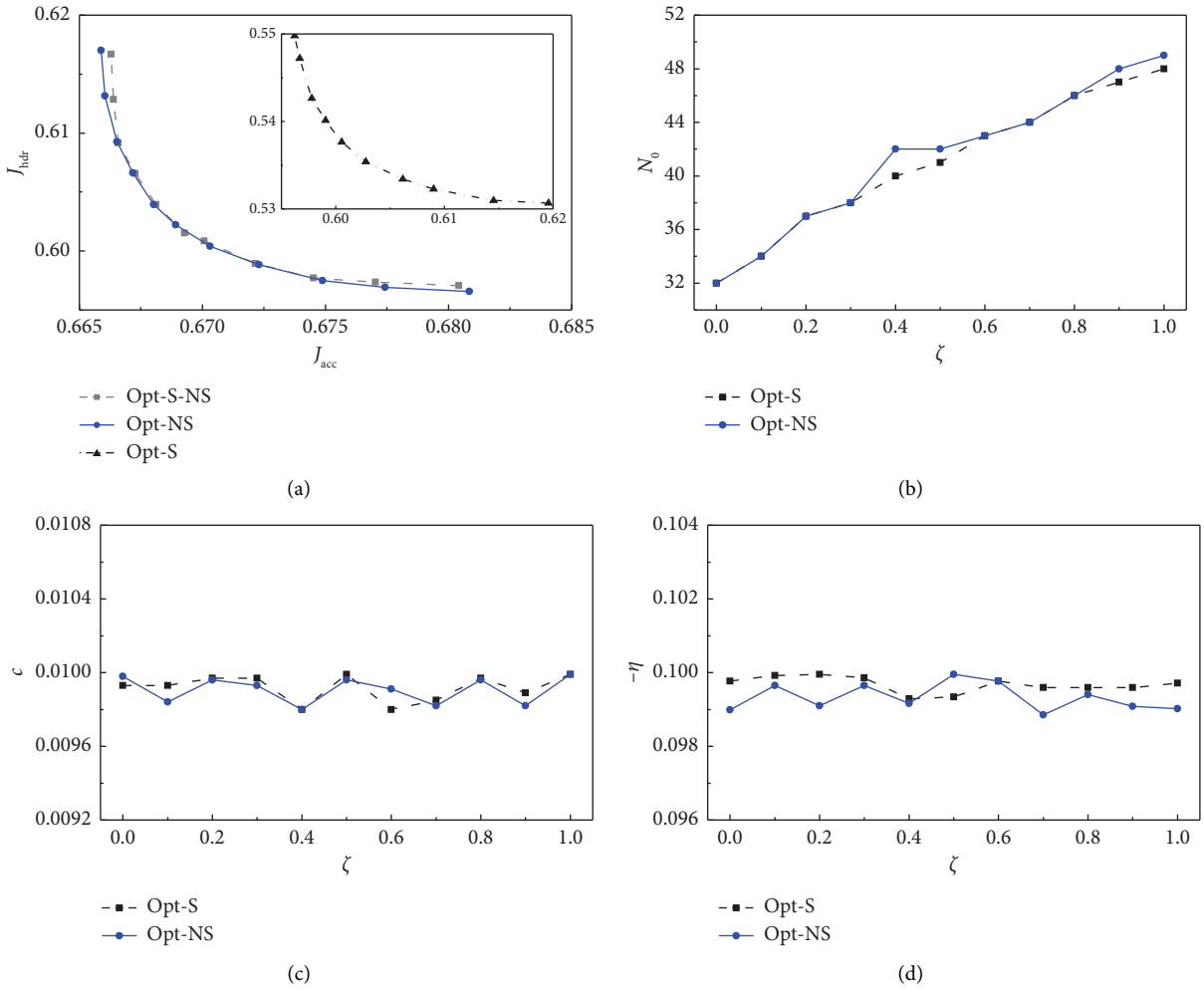

FIGURE 10: Optimal results for N&C. (a) Pareto front of performance indexes. (b) Optimal outrigger position. (c) Optimal outrigger damping coefficient. (d) Optimal negative stiffness ratio.

($\zeta = 0.5$). Figure 14 shows the objectives of the maximum normalized harmful drift ratio and floor absolute acceleration of three damped outrigger systems against maximum allowable negative stiffness ratio, respectively. Again, the N&C and C&N systems, particularly the N&C system, have been shown to be more effective in reducing harmful interstory drift and floor acceleration within limited amount of negative stiffness ratio, while the DN system could have the best performance with sufficient amount of negative stiffness ratio.

The above investigations suggest that the proposed combined NSDO and CDO damped outrigger system could provide valuable design flexibilities with damped outrigger configurations tailored for various objectives: (1) with adequate negative stiffness devices that do not cause the system to become unstable, the DN system would be the best design option by bringing down structure responses; (2) with limited amount negative stiffness devices, the N&C system would be the optimal configuration for its best utilization of devices, followed by the C&N and DN systems; and (3) when the available amount of negative stiffness devices lies in between, there might be a trade-offbetween the DN and N&C systems depending on the weightsassociated with harmful interstory drift and floor absolute acceleration.

5. Comparisons of the Efficiency of Different Outrigger Systems

To show the efficiency of the proposed stochastic optimization method for designing different outrigger systems in reducing earthquake-induced vibration as well as the potentials of the proposed combined NDO and CDO systems, the optimal designs of such systems obtained from last section are further examined under real earthquake records. Specifically, the optimal configurations of four damped outrigger systems with the weight equal to 0.5 and with total maximum absolute negative stiffness ratio being 0.1 (0.2 for the original DN system) are selected as examples for further evaluating their performance regarding time history response and energy distribution under typical real earthquake records as well as near-fault earthquake response envelopes. Note that the weight being 0.5 means that the structural acceleration is assumed to be as important as harmful drift ratio. The detailed parameters based on dual-response

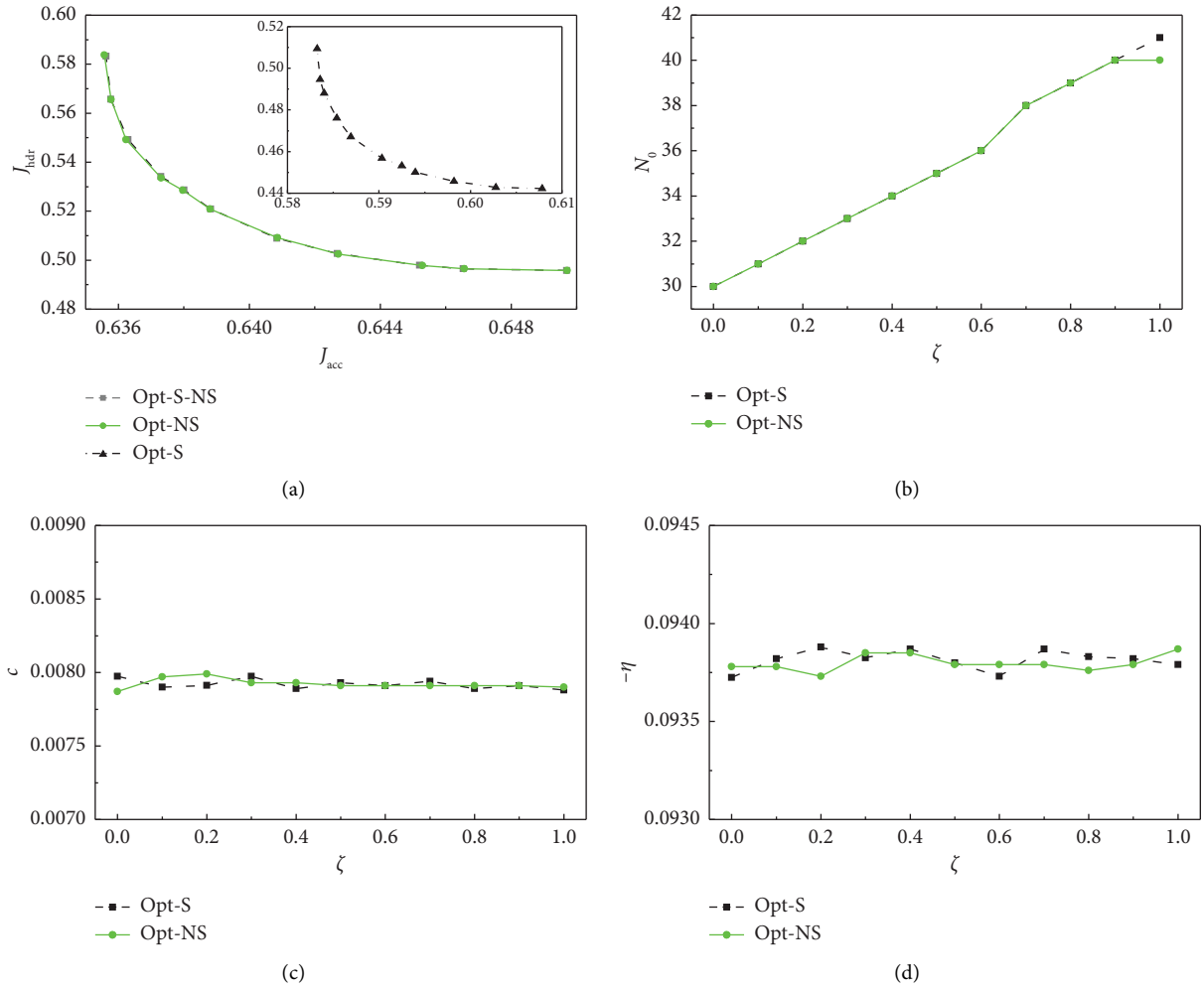

FIGURE 11: Optimal results for DN. (a) Pareto front of performance indexes. (b) Optimal outrigger position. (c) Optimal outrigger damping coefficient. (d) Optimal negative stiffness ratio.

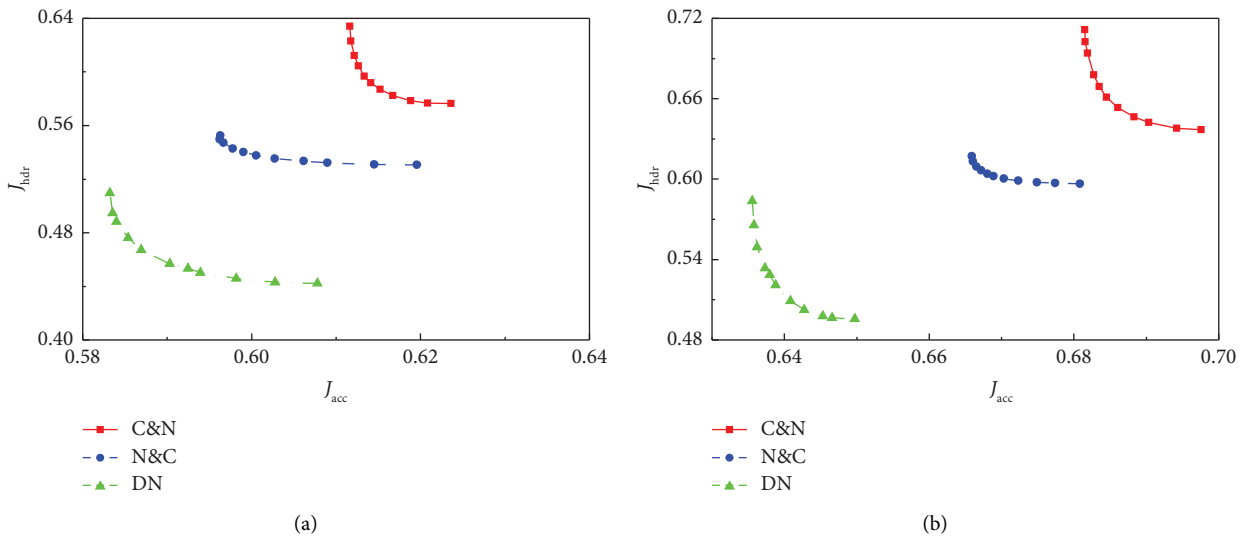

FIGURE 12: Pareto front for different outrigger systems. (a) Stationary-based optimal design. (b) Nonstationary-based optimal design.

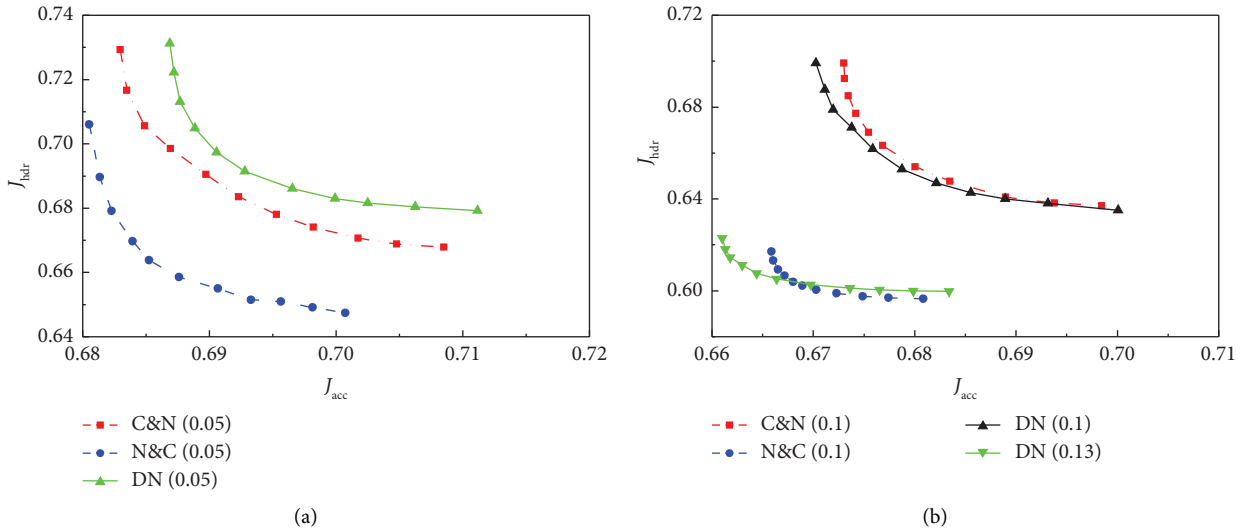

FIGURE 13: Pareto optimal fronts with different total negative stiffness ratio ($-\eta$). (a) 0-0.05. (b) 0-0.1 (0.13 only for the DN system).

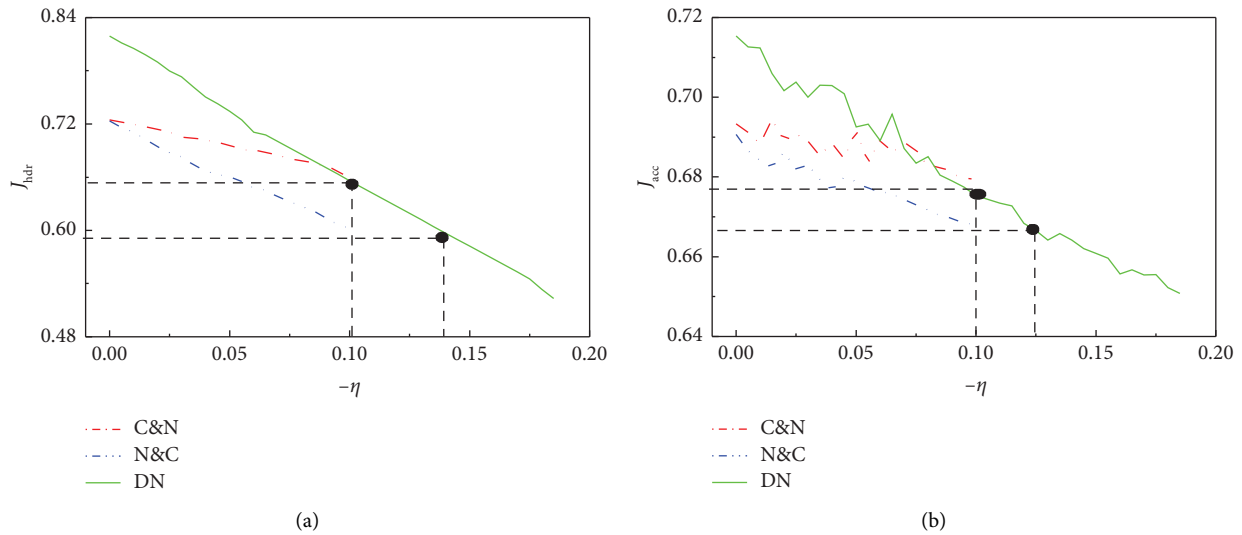

FIGURE 14: Influences of total normalized negative stiffness ratio ($-\eta$) at weight $\zeta = 0.5$. (a) Harmful drift ratio. (b) Acceleration.

criterion are listed in Table 2, where DN (0.1) represents the results of the DN system with the maximum total absolute negative stiffness ratio being 0.1, which is the same level as the C&N and N&C systems in the table. Such amount of limited negative stiffness ratio is chosen to show the competitiveness of the C&N and N&C systems, which could outperform the DN system with smaller negative stiffness ratio (see Figure 14), i.e., the proposed C&N and N&C systems are competitive with the DN system given the same negative stiffness ratio even in the worst scenario, and consequently the potentials of applying the C&N and N&C systems are evidenced.

5.1. Time History Response. In this section, the obtained optimal designs of different outrigger systems are further examined for structures under El Centro and Kobe records. Figure 15 shows the time history records of El Centro and Kobe on the left column and the corresponding power spectrum densities on the right with the peak ground acceleration adjusted to 0.35 g.

TABLE 2: Detailed parameters based on dual-response criterion.

Parameter	C&N	N&C	DN	DN (0.1)
η	−0.09822	−0.09995	−0.09379	−0.04945
c	0.00993	0.00996	0.00791	0.00989
N_0	40	42	35	42

The reduction ratios of the different outrigger systems using stochastic optimization approach in comparison with the BS under typical earthquake records are summarized in Table 3, and the corresponding time history curves of structural bottom story drift ratio and top peak acceleration are presented in Figures 16 and 17. From both the table and figures, all four damped outrigger systems

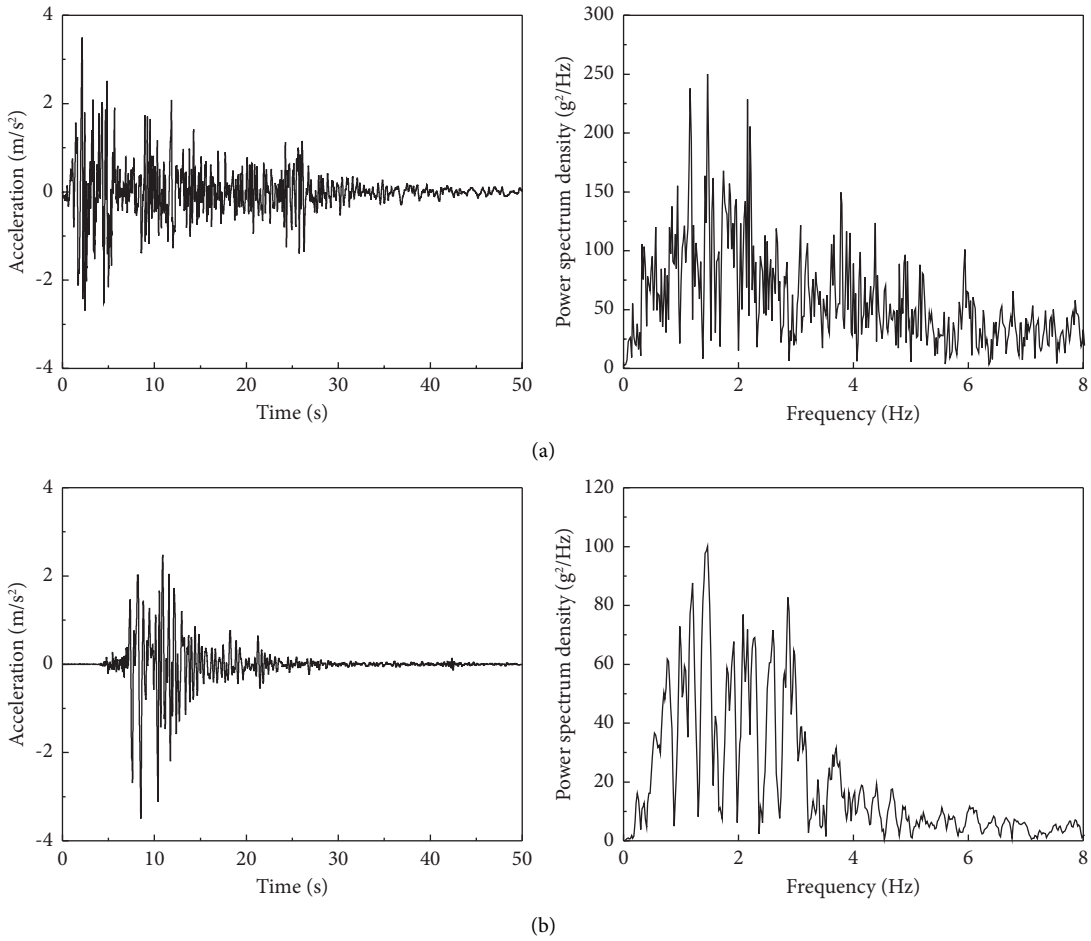

Figure 15: Acceleration and frequency-amplitude relationships for earthquake records. (a) El Centro. (b) Kobe.

Table 3: Control results of structural RMS response subjected to different seismic excitation.

Outrigger systems (OS)	Reduction ratio λ (%)					
	Bottom interstory drift RMS			Top acceleration RMS		
	El Centro	Kobe	Average	El Centro	Kobe	Average
C&N	49.39	40.48	44.94	29.02	36.41	32.72
N&C	55.84	43.54	49.69	31.12	35.87	33.49
DN	62.03	48.12	55.08	36.59	45.35	40.97
DN (0.1)	52.55	42.16	47.36	30.06	34.81	32.44

λ is the percentage reduction of the RMS response of different outrigger systems compared to the BS, i.e., $\lambda = BS\text{Response} - OS\text{Response}/BS\text{Response}$, where OS refers to four outrigger systems in the table.

could reduce the maximum harmful drift and floor acceleration significantly, with an average reduction of 45%–55% in the former and 32%–41% in the latter in comparison with the BS. Compared to other outrigger systems, the DN system with adequate negative stiffness devices has the best performance both in harmful interstory drift ratio and floor absolute acceleration. Additionally, while the both mixed damped outrigger systems have compatible reduction effect in terms of acceleration, the N&C system performs slightly better than the DN (0.1) and C&N systems with the same amount of negative stiffness devices, where the variation of vibration reduction is due to the variation of frequency content of the specific earthquake records.

5.2. Seismic Energy Distribution. As the damped outrigger systems are using the dampers as energy dissipation devices, it is natural to analyze the energy distribution of the systems. From the energy balance perspective, the seismic input energy E_I to the systems when the main structures remain linear is transformed into kinetic energy E_K, strain energy E_S, and the dissipated energy both by inherent damping E_C and the installed dampers E_D, i.e., $E_K + E_S + E_C + E_D = E_I$. As opposed to the typical analysis only focusing on the energy dissipated by dampers, the dampers installed affect not only the dissipated energy, but also the input energy, or to put it this way, the purpose of installing dampers is to protect the main structure, i.e., the actual concern of seismic input energy influencing the systems' behavior is $(E_K + E_S)$. Therefore, the quantity $(E_I - E_C - E_D)$ is a more meaningful performance index rather than E_D itself.

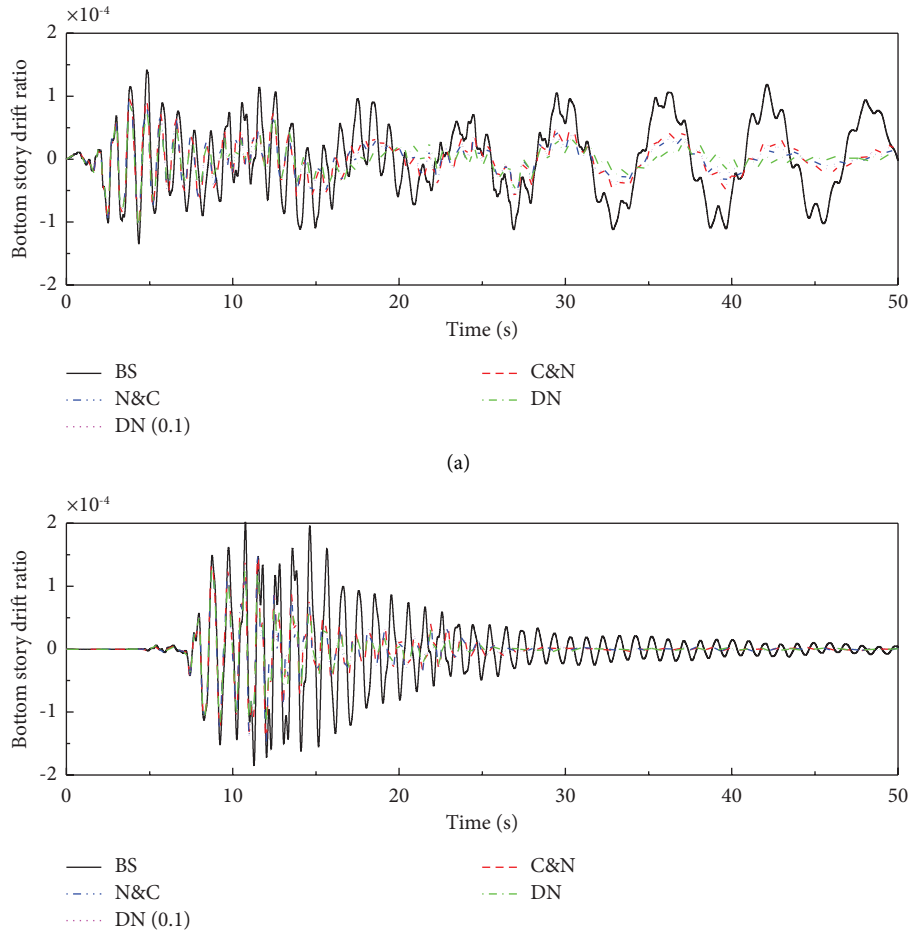

Figure 16: Comparison of time history curves of bottom story drift ratio of different outrigger systems under typical earthquake. (a) El Centro. (b) Kobe.

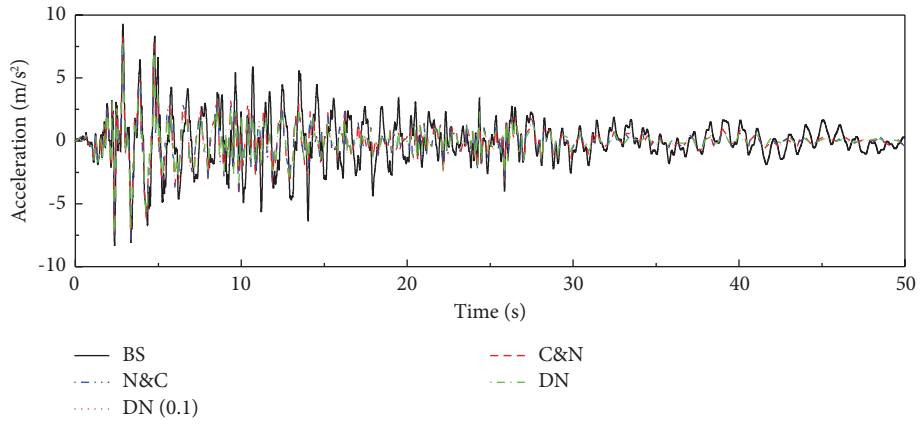

Figure 17: Continued.

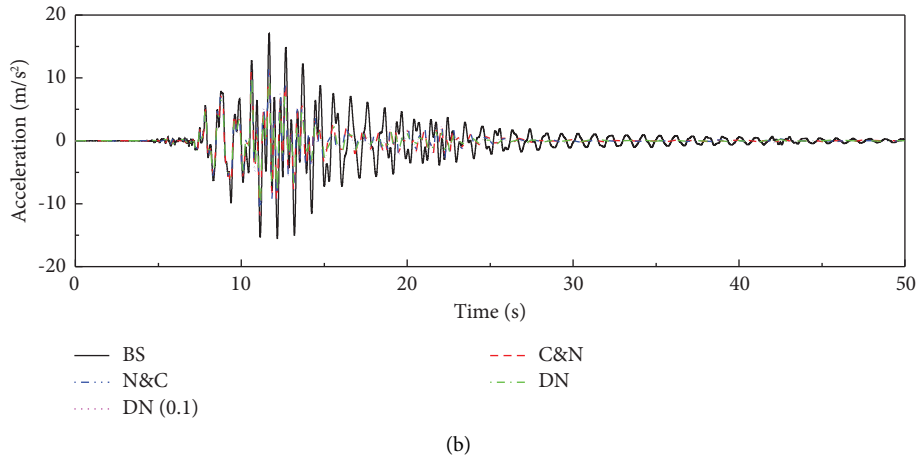

(b)

Figure 17: Comparison of time history curves of structural top acceleration of different outrigger systems under typical earthquake. (a) El Centro. (b) Kobe.

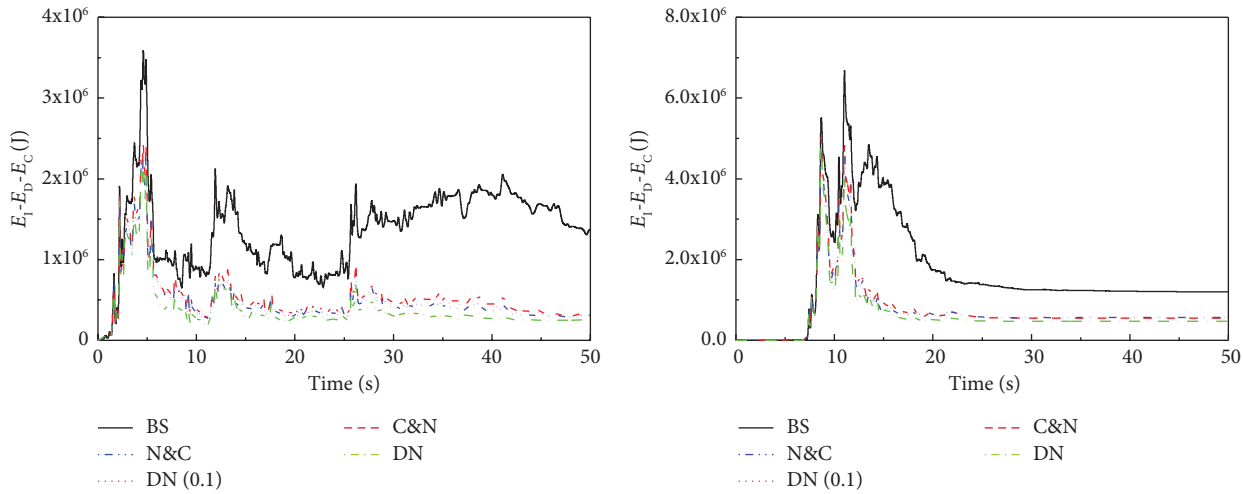

(a) (b)

Figure 18: Energy dissipation with different outrigger systems under typical earthquake records. (a) El Centro. (b) Kobe.

Again, the significant seismic performance of four damped outrigger systems is evidenced by Figure 18, which shows how the energy quantities $(E_I - E_C - E_D)$ of different outrigger systems evolve during earthquakes, and by Table 4 that summarizes the corresponding maximum energy that could damage the target main structures. Compared to BS structure, the DN system cut the main structure energy input by around 39% and 27% under El Centro and Kobe records, respectively, as opposed to 36% and 25% for the N&C system, respectively, which has slightly better performance than the DN (0.1) and C&N systems.

5.3. Seismic Response Envelopes. To evaluate the response envelopes of different outrigger systems, 28 near-fault earthquake records are selected [59]. Figure 19 presents the response spectra of these selected records. Comparisons of mean response envelopes by different outrigger systems under selected earthquake records are given in Figure 20.

Table 4: Maximum energy dissipation under selected earthquake records.

Outrigger systems	El Centro $E_I - E_D - E_C$ (e^6J)	Kobe $E_I - E_D - E_C$ (e^6J)
BS	3.5935	6.6775
C&N	2.4504	5.0661
N&C	2.2962	4.9841
DN	2.2011	4.8466
DN (0.1)	2.3319	5.0219

Compared to BS structure, C&N, N&C, DN, and DN (0.1) can reduce the average value of the structural maximum harmful story drift ratio by 19.26%, 20.34%, 25.89%, and 19.63% and absolute acceleration by 20.27%, 22.56%, 30.61%, and 20.48%, respectively. Such result is consistent with the previous analysis, i.e., the D&N system has the best performance, followed by the N&C, DN (0.1), and C&N systems which have similar performance levels.

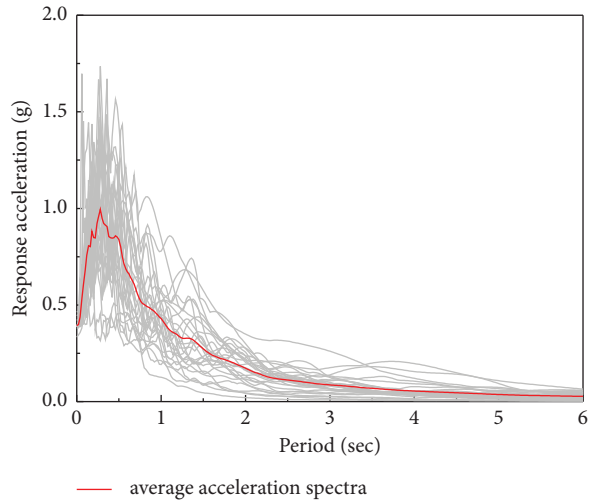

Figure 19: Response spectra of the selected seismic records.

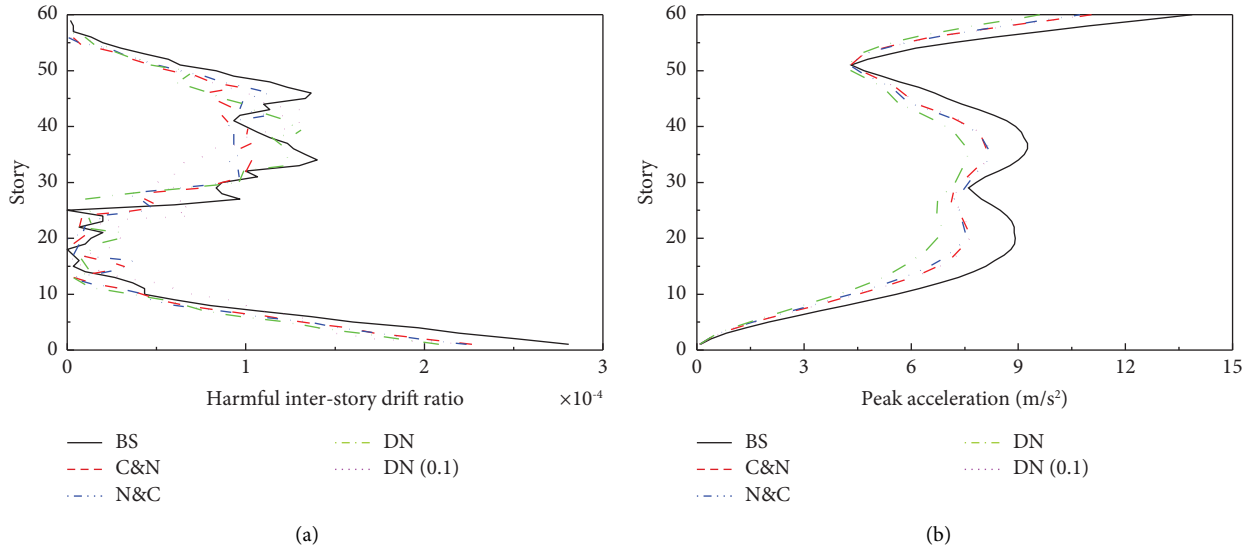

Figure 20: Comparisons of mean response envelopes by different outrigger systems under selected earthquake records. (a) Harmful interstory ratio. (b) Peak acceleration.

6. Conclusions

This paper proposed a stochastic optimization method to investigate optimal configurations of combined negative stiffness damped outriggers (NSDOs) and conventional damped outriggers (CDOs) subjected to nonstationary stochastic seismic excitation. The simplified analysis model of various combinations of damped outriggers was developed, and the state-space representation of outrigger systems was formulated. The nonstationary seismic excitation was modeled as a uniformly modulated stationary Gaussian process with a time-modulating function following Clough–Penzien spectrum. Combining equations of motions of outrigger systems and seismic excitation gave rise to the augmented state-space representation of structure-damper-excitation and subsequently the differential Lyapunov equation. The optimal designs of damped outriggers were defined via the solution of the differential Lyapunov equation. The multiobjective optimization with Pareto optimal fronts was adopted to deal with conflicting objectives. The sensitivity of negative stiffness ratio on the design objectives of reducing maximum harmful interstory drift and floor absolute acceleration was studied. The efficacy of the proposed method was demonstrated through a tall building designed with various damped outriggers, and the optimal designs were further examined under real earthquake records. These investigations showed the following:

(1) The proposed multiobjective optimization method incorporated uniformly modulated Clough–Penzien filter to model nonstationary stochastic seismic excitation and Pareto optimal fronts to deal with conflicting objectives, whereby the designs of the combined negative stiffness damped outrigger and

conventional damped outrigger systems were optimized. The efficacy of the proposed method was verified through an illustrated example.

(2) The proposed method was applied to optimally design the proposed combined NSDO and CDO systems subjected to nonstationary seismic excitation. With this method, the obtained optimal parameters of dampers and outrigger arrangement for such systems could reduce around 36%–50% in maximum RMS values of harmful interstory drift ratio and over 30% in peak RMS values of floor absolute acceleration compared to the bare structure (BS). Provided with sufficient negative devices, the double negative stiffness outrigger (DN) system performed the best, followed by the two combined systems, the N&C and C&N systemswithin which the NSDO is correspondingly placed above and below the CDO.

(3) Stochastic optimizations of three damped outrigger systems considering nonstationary and stationary seismic excitations were compared, and the stationary-based optimization was further evaluated under nonstationary excitation. Although the stationary assumption of seismic excitation could lead to overestimation of structural responses with respect to both harmful interstory drift and floor acceleration, both the optimal designs of three damped outrigger systems between stationary and nonstationary earthquakesand the deviations in optimal objectivevalues using the stationary and nonstatoinary earthquakes-based optimal designs were less than 2%. Such findings justify that the less time-consumingstationary-based seismic optimization is adequate for engineering design practice.

(4) The sensitivity analysis was conducted by analyzing the stochastic optimization results with respect to the maximum allowable negative stiffness ratio. The DN system would be the best design option provided with adequate negative stiffness devices that do not cause the system to become unstable, while the N&C system would be the optimal configuration for its best utilization of devices with limited amount negative stiffness devices. When the available amount of negative stiffness devices lies in between, there might be a trade-offbetween the N&C and DN systems depending on the weights associatedwithharmful interstory drift and floor absolute acceleration. Therefore, the proposed combined NSDO and CDO damped outrigger systems could provide valuable design flexibilities with damped outrigger configurations tailored for various objectives.

(5) The optimal designs of damped outrigger systems using the proposed optimization method were further examined under typical as well as near-fault earthquake records. With emphasis both on harmful drift and floor acceleration, the optimal designs of four damped outrigger systems were evaluated regarding time history dynamic response, energy distribution, and response envelopes. Compared to BS, all damped outrigger systems on average could reduce the harmful interstory drift by 45%–55% and floor absolute acceleration by 32%–41% as well as reduce the energy input to the main structures by 25%–39% under El Centro and Kobe earthquake records; however, such reduction effect in the case of near-fault earthquakes decreased to 19%–26% and 20%–31% in terms of average response envelopes, respectively.

Data Availability

The data used to support the findings of this study are available from the corresponding author upon request.

Conflicts of Interest

The authors declare that they have no conflicts of interest.

Acknowledgments

The authors greatly acknowledge the financial support from the National Natural Science Foundation of China (grant no. 51878274) and Academic Degrees & Graduate Education Reform Project of Henan Province (2021SJGLX015Y). The corresponding author also gratefully acknowledges the support from the Special Program of Guangdong Science and Technology in 2021 (grant no. 210715155861712) and the guidance from Prof. Quang Wang of Shantou University.

References

[1] J. R. Wu and Q. S. Li, "Structural performance of multi-outrigger-braced tall buildings," *The Structural Design of Tall and Special Buildings*, vol. 12, no. 2, pp. 155–176, 2003.

[2] B. S. Smith and I. Salim, "Parameter study of outrigger-braced tall building structures," *Journal of the Structural Division*, vol. 107, no. 10, pp. 2001–2014, 1981.

[3] J. Lee, M. Bang, and J.-Y. Kim, "An analytical model for high-risewall-frame structures with outriggers," *The Structural Design of Tall and Special Buildings*, vol. 17, no. 4, pp. 839–851, 2008.

[4] R. Smith, R. Merello, and M. Willford, "Intrinsic and supplementary damping in tall buildings," *Proceedings of the Institution of Civil Engineers - Structures and Buildings*, vol. 163, no. 2, pp. 111–118, 2010.

[5] B. G. Kavyashree, S. Patil, and V. S. Rao, "Evolution of outrigger structural system: a state-of-the-art review," *Arabian Journal for Science and Engineering*, vol. 46, no. 11, pp. 10313–10331, 2021.

[6] Y. Zhou, L. Xing, and G. Zhou, "Spectrum analysis-based model for the optimal outrigger location of high-rise buildings," *Journal of Earthquake Engineering*, vol. 25, no. 12, pp. 2406–2431, 2019.

[7] T. Asai, Y. Terazawa, T. Miyazaki, P. C. Lin, and T. Takeuchi, "First mode damping ratio oriented optimal design procedure for damped outrigger systems with additional linear viscous dampers," *Engineering Structures*, vol. 247, p. 247, 2021.

[8] L. Xing, Y. Zhou, and M. Aguaguiña, "Optimal outrigger locations of double-pure-outrigger systems and combined

energy-dissipating outrigger systems under seismic loads," *Soil Dynamics and Earthquake Engineering*, vol. 153, Article ID 107121, 2022.

[9] R. J. Smith and M. R. Willford, "The damped outrigger concept for tall buildings," *The Structural Design of Tall and Special Buildings*, vol. 16, no. 4, pp. 501–517, 2007.

[10] M. Willford, R. Smith, D. Scott, and M. Jackson, "Viscous dampers come of age," *Structures Magazine*, vol. 6, pp. 15–18, 2008.

[11] Z. Lu, X. He, and Y. Zhou, "Performance-based seismic analysis on a super high-rise building with improved viscously damped outrigger system," *Structural Control and Health Monitoring*, vol. 25, no. 8, p. e2190, 2018.

[12] H. Jiang, S. Li, and Y. Zhu, "Seismic performance of high-rise buildings with energy-dissipation outriggers," *Journal of Constructional Steel Research*, vol. 134, pp. 80–91, 2017.

[13] J. M. Ding, S. Y. Wang, and H. L. Wu, "Seismic performance analysis of viscous damping outrigger in super high-rise buildings," *The Structural Design of Tall and Special Buildings*, vol. 27, no. 13, p. e1486, 2018.

[14] H. S. Kim and J. W. Kang, "Smart outrigger damper system for response reduction of tall buildings subjected to wind and seismic excitations," *International Journal of Steel Structures*, vol. 17, no. 4, pp. 1263–1272, 2017.

[15] M. Wang, S. Nagarajaiah, and F.-F. Sun, "Optimal design of supplemental negative stiffness damped outrigger system for high-rise buildings resisting multi-hazard of winds and earthquakes," *Journal of Wind Engineering and Industrial Aerodynamics*, vol. 218, Article ID 104761, 2021.

[16] Z.-Q. Chen and Z.-H. Wang, "A novel passive energy dissipation system for frame-core tube structure," in *Proceedings of the The Seventh Asia-Pacific Conference on Wind Engineering*, Taipei, Taiwan, 2009.

[17] Y. Chen, D. M. McFarland, Z. Wang, B. F. Spencer, and L. A. Bergman, "Analysis of tall buildings with damped outriggers," *Journal of Structural Engineering*, vol. 136, no. 11, pp. 1435–1443, 2010.

[18] P. Tan, C. J. Fang, and F. L. Zhou, "Dynamic characteristics of a novel damped outrigger system," *Earthquake Engineering and Engineering Vibration*, vol. 13, no. 2, pp. 293–304, 2014.

[19] C. J. Fang, P. Tan, C. M. Chang, and F. L. Zhou, "A general solution for performance evaluation of a tall building with multiple damped and undamped outriggers," *The Structural Design of Tall and Special Buildings*, vol. 24, no. 12, pp. 797–820, 2015.

[20] P. Tan, C. J. Fang, C. M. Chang, B. F. Spencer, and F. L. Zhou, "Dynamic characteristics of novel energy dissipation systems with damped outriggers," *Engineering Structures*, vol. 98, pp. 128–140, 2015.

[21] M. P. Singh, N. P. Verma, and L. M. Moreschi, "Seismic analysis and design with Maxwell dampers," *Journal of Engineering Mechanics*, vol. 129, no. 3, pp. 273–282, 2003.

[22] Y. T. Chen and Y. H. Chai, "Effects of brace stiffness on performance of structures with supplemental Maxwell model-based brace–damper systems," *Earthquake Engineering & Structural Dynamics*, vol. 40, no. 1, pp. 75–92, 2011.

[23] C. Li, T. Li, D. Ban, and X. Ge, "Equivalent damping of SDOF structure with Maxwell damper," *Earthquake Engineering and Engineering Vibration*, vol. 17, no. 3, pp. 627–639, 2018.

[24] L. Chen, L. Sun, and S. Nagarajaiah, "Cable with discrete negative stiffness device and viscous damper: passive realization and general characteristics," *Smart Structures and Systems*, vol. 15, no. 3, pp. 627–643, 2015.

[25] C. Qu, H.-N. Li, L. Huo, and T.-H. Yi, "Optimum value of negative stiffness and additional damping in civil structures," *Journal of Structural Engineering*, vol. 143, no. 8, Article ID 04017068, 2017.

[26] P. Zhou and H. Li, "Modeling and control performance of a negative stiffness damper for suppressing stay cable vibrations," *Structural Control and Health Monitoring*, vol. 23, no. 4, pp. 764–782, 2016.

[27] M. Wang, F. F. Sun, and S. Nagarajaiah, "Simplified optimal design of MDOF structures with negative stiffness amplifying dampers based on effective damping," *The Structural Design of Tall and Special Buildings*, vol. 28, no. 15, p. e1664, 2019.

[28] Z. Wang, Z. Cheng, H. Wang, F. Yue, H. Gao, and B. Fan, "Damping of a stay cable with two eddy-current inertial mass dampers: theoretical Analysis, experimental study, and parameter Optimization," *Structural Control and Health Monitoring*, vol. 29, p. e3085, 2022.

[29] X. Shi and S. Zhu, "A comparative study of vibration isolation performance using negative stiffness and inerter dampers," *Journal of the Franklin Institute*, vol. 356, no. 14, pp. 7922–7946, 2019.

[30] H. Li, J. Li, and K. Bi, "A quasi-active negative stiffness damper for structural vibration control under earthquakes," *Mechanical Systems and Signal Processing*, vol. 173, Article ID 109071, 2022.

[31] M. Wang, S. Nagarajaiah, and F. F. Sun, "Dynamic characteristics and responses of damped outrigger tall buildings using negative stiffness," *Journal of Structural Engineering*, vol. 146, no. 12, Article ID 04020273, 2020.

[32] C. J. Fang, "Applicability of damped outrigger systems using timoshenko beam theory," *International Journal of Structural Stability and Dynamics*, vol. 22, no. 6, Article ID 2250076, 2022.

[33] C. J. Fang, B. F. Spencer, J. Q. Xu, P. Tan, and F. L. Zhou, "Optimization of damped outrigger systems subject to stochastic excitation," *Engineering Structures*, vol. 191, pp. 280–291, 2019.

[34] F.-F. Sun, M. Wang, and S. Nagarajaiah, "Multi-objective optimal design and seismic performance of negative stiffness damped outrigger structures considering damping cost," *Engineering Structures*, vol. 229, Article ID 111615, 2021.

[35] K. Park, D. Kim, D. Yang, D. Joung, I. Ha, and S. Kim, "A comparison study of conventional construction methods and outrigger damper system for the compensation of differential column shortening in high-rise buildings," *International Journal of Steel Structures*, vol. 10, no. 4, pp. 317–324, 2010.

[36] M. Jackson and D. M. Scott, "Increasing efficiency in tall buildings by damping," in *Proceedings of the Structures Congress 2010*, Orlando, Florida, 2010.

[37] L. Chen, Z. Liu, S. Nagarajaiah, L. Sun, L. Zhao, and W. Cui, "Vibration mitigation of long-span bridges with damped outriggers," *Engineering Structures*, vol. 271, Article ID 114873, 2022.

[38] J. Chen, F. Kong, and Y. Peng, "A stochastic harmonic function representation for non-stationary stochastic processes," *Mechanical Systems and Signal Processing*, vol. 96, pp. 31–44, 2017.

[39] Z. Liu, W. Liu, and Y. Peng, "Random function based spectral representation of stationary and non-stationary stochastic processes," *Probabilistic Engineering Mechanics*, vol. 45, pp. 115–126, 2016.

[40] F. Kong, R. Han, S. Li, and W. He, "Non-stationary approximate response of non-linear multi-degree-of-freedom systems subjected to combined periodic and stochastic

excitation," *Mechanical Systems and Signal Processing*, vol. 166, Article ID 108420, 2022.

[41] H. Iemura and M. H. Pradono, "Application of pseudo-negative stiffness control to the benchmark cable-stayed bridge," *Journal of Structural Control*, vol. 10, no. 3-4, pp. 187–203, 2003.

[42] F. Weber and H. Distl, "Semi-active damping with negative stiffness for multi-mode cable vibration mitigation: approximate collocated control solution," *Smart Materials and Structures*, vol. 24, no. 11, Article ID 115015, 2015.

[43] D. T. R. Pasala, A. A. Sarlis, S. Nagarajaiah, A. M. Reinhorn, M. C. Constantinou, and D. Taylor, "Adaptive negative stiffness: new structural modification approach for seismic protection," *Journal of Structural Engineering*, vol. 139, no. 7, pp. 1112–1123, 2013.

[44] Z. H. Wang, Z. P. Cheng, G. Z. Yin, and W. A. Shen, "A magnetic negative stiffness eddy-current inertial mass damper for cable vibration mitigation," *Mechanical Systems and Signal Processing*, vol. 188, Article ID 110013, 2023.

[45] Y. C. Wang and R. S. Lakes, "Stable extremely-high-damping discrete viscoelastic systems due to negative stiffness elements," *Applied Physics Letters*, vol. 84, no. 22, pp. 4451–4453, 2004.

[46] H. Iemura and M. H. Pradono, "Advances in the development of pseudo-negative-stiffness dampers for seismic response control," *Innovative Infrastructure Solutions*, vol. 7, no. 1, pp. 1–15, 2022.

[47] J. N. Yang, A. K. Agrawal, B. Samali, and J. C. Wu, "Benchmark problem for response control of wind-excited tall buildings," *Journal of Engineering Mechanics*, vol. 130, no. 4, pp. 437–446, 2004.

[48] L. K. Liu, P. Tan, H. T. Ma, W. M. Yan, and F. L. Zhou, "A novel energy dissipation outrigger system with rotational inertia damper," *Advances in Structural Engineering*, vol. 21, no. 12, pp. 1865–1878, 2018.

[49] S. R. Gunakala, D. Comissiong, K. Jordan, and A. Sankar, "A finite element solution of the beam equation via MATLAB," *International Journal of Applied*, vol. 2, no. 8, 2012.

[50] L. Liu, X. Li, P. Tan, Z. Pan, and S. Zhang, "Damping performance analysis of the damped outrigger system based on H," *International Journal of Structural Stability and Dynamics*, vol. 22, no. 13, Article ID 2250149, 2022.

[51] D. De Domenico and G. Ricciardi, "Optimal design and seismic performance of tuned mass damper inerter (TMDI) for structures with nonlinear base isolation systems," *Earthquake Engineering & Structural Dynamics*, vol. 47, no. 12, pp. 2539–2560, 2018.

[52] Y. Wen, F. Gomez, D. Li, and B. F. Spencer Jr, "Generalized optimal design of multiple tuned inerter dampers for control of MDOF structures under stochastic seismic excitation," *Structural Control and Health Monitoring*, vol. 29, no. 1, p. e2853, 2022.

[53] C. S. Gb50011, *Code for Seismic Design of Buildings*, China Building Industry Press, Beijing, 2010.

[54] J. Cai, G. Bu, C. Yang, Q. Chen, and Z. Zuo, "Calculation methods for inter-story drifts of building structures," *Advances in Structural Engineering*, vol. 17, no. 5, pp. 735–745, 2014.

[55] T. G. Kolda, R. M. Lewis, and V. Torczon, "Optimization by direct search: new perspectives on some classical and modern methods," *SIAM Review*, vol. 45, no. 3, pp. 385–482, 2003.

[56] M. Torbol, H. Gomez, and M. Feng, "Fragility analysis of highway bridges based on long-term monitoring data," *Computer-Aided Civil and Infrastructure Engineering*, vol. 28, no. 3, pp. 178–192, 2013.

[57] Y. L. Xu, Q. He, and J. Ko, "Dynamic response of damper-connected adjacent buildings under earthquake excitation," *Engineering Structures*, vol. 21, no. 2, pp. 135–148, 1999.

[58] J. Xu, B. F. Spencer Jr, X. Lu, X. Chen, and L. Lu, "Optimization of structures subject to stochastic dynamic loading," *Computer-Aided Civil and Infrastructure Engineering*, vol. 32, no. 8, pp. 657–673, 2017.

[59] Applied Technology Council, *Quantification of Building Seismic Performance Factors*, US Department of Homeland Security FEMA, Washington, DC, USA, 2009.